Award Title: TAS: :89 0227: :TAS Recovery Act - Optimization and Control of Electric Power Systems

SuperOPF and Incorporation of Transient Stability Constrints into OPF.

Final Report

Prof. Hsiao-Dong Chiang
Dr. Ray D. Zimmerman
Prof. Robert J. Thomas

School of Electrical Engineering
Cornell University
Ithaca, NY 14853

December 12, 2013

Contents

1 Introduction 7

2 Single Period SuperOPF 10

2.1 Nomenclature 12

2.2 Stage 1 - Day-Ahead Problem 13

2.3 Stage 2 - Real-Time Adjustment of Dispatch 17

2.3.1 Redispatching the Intact System 17

2.3.2 Redispatching in a Post-Contingency State 18

3 Multi-period SuperOPF 20

3.1 Introduction 20

3.2 Relation to Control Problem 23

3.3 Nomenclature 24

3.4 Formulation 28

3.5 Value of Residual Storage 35

3.6 Problem Decomposition 43

4 Evaluation Study of the Incorporation of Transient Stability Constraints into Optimal Power Flow 47

4.1 Introduction. 47

4.2 TSOPF Problem Formulations. 47

4.2.1 Conventional OPF Formulation 48

4.2.2 Transient Stability Constraints 48

4.3 Proxi for Transient Stability Constraints and Numerical Issues . . . 51

4.4 Method for Computing Exact Threshold 52

4.5 Proxi from Stability Region Viewpoint. 53

4.6 Numerical Study on Threshold Values 58

4.6.1 Underestimate of Threshold and CCT 59

4.6.2 Overestimate of Threshold and CCT 60
4.7 Accurate Thresholds under Different Conditions. 61
4.7.1 Type of Contingencies 61
4.7.2 Loading Conditions 62
4.7.3 Severe Contingencies 64
4.8 TSCOPF using Different Threshold Values 64
4.9 Conclusion 65
5 A Novel BCU-Based OPF Method for Large-Scale Power Systems with Transient Stability Constraints 66
5.1 Introduction. 66
5.2 TSCOPF Problem Formulations 67
5.2.1 Objective Function 67
5.2.2 Conventional OPF equality and inequality constraints 67
5.2.3 Transient Stability Constraints 68
5.3 Controlling Unstable Equilibrium Point 71
5.4 A BCU-Based Scheme for Computing Threshold 73
5.5 Proposed BCU-based TSCOPF Method 76
5.6 Case Studies. 79
5.7 Conclusions 82
References 83

List of Figures

2-1 Graphical Representation of Co-optimization Structure 11

2-2 Contract, Incs/Decs and Reserve 12

3-1 Overall Problem Structure 35

3-2 Problem Decomposition 43

4-1 The sustained fault-on trajectory $x_f(t)$, starting from the pre-fault SEP x_s^{pre} , moves toward the stability boundary $\partial A(x_s^{post})$ and intersects it at the exit point, x_e . x_s^{pre} is assumed to lie inside the stability region of post-fault SEP $A(x_s^{post})$. 50

4-2 The exact threshold value can be obtained at the highest peak of the critically stable post-fault trajectory. The fault-on trajectory crosses the stability boundary at the critical clearing time of 0.2429 second 54

4-3 Critically stable swing curves when clearing time is 0.2429 second, slightly less than the CCT. The peak of the rotor angles is observed at 2.9 radian or 166.16°. 55

4-4 A stable trajectory travelling inside the stability region in the state space, while an unstable trajectory lying outside the stability region moves away from it. 55

4-5 The stable swing curves and unstable stable swing curves in Figure 4-2 as a function of time. The exact threshold value of 2.9

radians of 166.16 degrees was found at CCT = 0.2429 second by an exact method, and compared to the commonly used threshold of 100°. 56

4-6 At fault clearing time = 0.1420 second, a stable post-fault trajectory is confined in the correct limits of +/- 177.62°. 56

4-7 At fault clearing time = 0.110 sec, a stable post-fault trajectory is confined in the commonly used limits of +/- 100°. 57

4-8 Fault clearing time = 0.1420 sec, the post-fault trajectory converges to a post-fault SEP 57

4-9 A multi-swing unstable post-fault trajectory can take more than 15 seconds before encountering an angle separation. 58

5-1 The fault-on trajectory $x_f(t)$, starting from the pre-fault SEP x_s^{pre}, moves toward the stability boundary $\partial A(x_s^{post})$ and intersects it at the exit point, x_e. 69

5-2 Visualization of two initial points for computing system thresholds. Point 1 can be computed by time-domain-based while Point 2 by the proposed CUEP-based scheme. System thresholds computed from point 1 leads to an exact value while the results computed from point 2 are estimated and conservative values. 73

5-3 The conceptual BCU-based TSCOPF method for large-scale power systems with large contingency lists. The method consists of

(i) fast assessment and screening by BCU method for taking out irrelevant contingencies (ii) computation of system and contingency dependent threshold values via a BCU-base scheme, (iii) Reduce-space interior point method. 76

5-4 The flow chart of the BCU-based OPF method for solving large-scale TSCOPF problems with a large-size contingencies. 78

List of Tables

3-1 Five Price Model 41

4-1 CLEARING TIMES AND THE PEAKS OF POST-FAULT TRAJECTORIES. . . 53

4-2 Relative Error Percentage of Estimated CCT's 59

4-3 Exact Threshold Values in Different Types of Contingencies 61

4-4 Exact Values of Thresholds in Different Loading 63

4-5 Exact Values of Thresholds in Severe Contingencies 63

5-1 Exact (Time-domain) vs. Estimated (BCU) Threshold Values 74

5-2 Exact (Time-domain) vs. Estimated (BCU) CPU Time 75

5-3 Summary of All Test Systems. 79

5-4 BCU Classifiers and Screening performance. 80

5-5 Capability to handle large contingency lists Conventional TSCOPF 100° (IPM) vs. BCU-based TSCOPF (IPM) 80

5-6 TSCOPF Solution Quality Fixed threshold 100° vs. Computed Thresholds (BCU-based) 81

Chapter 1: Introduction

1-1. SuperOPF

The name SuperOPF is used to refer several projects, problem formulations and software tools intended to extend, improve and re-define some of the standard methods of optimizing electric power systems.

Our work included applying primal-dual interior point methods to standard AC optimal power flow problems of large size, as well as extensions of this problem to include co-optimization of multiple scenarios.

The original SuperOPF problem formulation was based on co-optimizing a base scenario along with multiple post-contingency scenarios, where all AC power flow models and constraints are enforced for each, to find optimal energy contracts, endogenously determined locational reserves and appropriate nodal energy prices for a single period optimal power flow problem with uncertainty. This led to example non-linear programming problems on the order of 1 million constraints and half a million variables.

The second generation SuperOPF formulation extends this by adding multiple periods and multiple base scenarios per period. It also incorporates additional variables and constraints to model load following reserves, ramping costs, and storage resources. While these enhancements to the formulation add the valuable new capability of addressing the uncertainty of both renewables and contingencies in a multi-period context with storage, they can easily lead to increases of two or three orders of magnitude in the problem size, highlighting the need for suitable decomposition and parallelization techniques for such problems.

The SuperOPF planning tool, based on a modified version the first generation SuperOPF utilizing a DC power flow model and incorporating optimal generation investment, is used to study and compare optimal investment paths under different environmental and economic policy assumptions for systems as large as the entire

Eastern Interconnect. Even with a highly reduced network model and limited number of load scenarios the problem easily reaches the order of a few million variables and constraints. Modifications have been made to this tool to facilitate a more adequate modeling of renewable sources of energy such as wind and solar. Adequately capturing the joint distributions of load and wind and solar availability requires a substantial increase in the number of representative hours used to represent the operating conditions throughout the year. The resulting problem is an extremely large scale LP problem that would benefit from advanced algorithms.

A third generation of the multi-period SuperOPF, adds both integer variables and a receding horizon framework in which the problem type is more challenging (mixed integer), the size is even larger, and it must be solved more frequently, pushing the limits of currently available algorithms and solvers.

Chapter 2 and Chapter 3 describe the problem formulations for the various SuperOPF problem types.

1-2. Incorporation of Transient Stability Constraints

The consideration of transient stability constraints in optimal power flow (OPF) problems has become increasingly important in modern power systems. Transient stability constrained OPF (TSCOPF) is a nonlinear optimization problem subject to a set of algebraic and differential equations. Solving a TSCOPF problem can be challenging due to (i) the differential-equation constraints in an optimization problem, (ii) the lack of a true analytical expression for transient stability in OPF. To handle the dynamics in TSCOPF, the set of differential equations can be approximated or converted into equivalent algebraic equations before they are included in an OPF formulation.

The direct discretization of the differential equations was proposed in [6], and utilized in [8]-[15]. This technique however is subject to inaccuracy and convergence issues due to the approximation and the introduction of large numbers of variables and equations for each time step. Therefore, the functional transformation technique was proposed in [7] to handle differential equations by converting the infinite-dimensional TSCOPF into a finite-dimensional optimization problem.

Mathematically, the transient stability of a power system does not have an analytical expression that can be directly incorporated in an OPF formulation. To avoid this difficulty, many researchers use a predefined and fixed threshold for rotor angles as a mean to determine transient stability of the system, see for example [6]-[16]. The value of the thresholds used in the literature usually varies from 100° to 120°, but the explanation on how it is selected is still lacking or nonexistent. Although this proxi may suffice as a simplified criterion, it is not an exact expression of transient stability in power system. Therefore, the results from using this proxi in TSCOPF may be subject to compromises and errors. In Chapter 4, a rigorous evaluation of using a predefined and fixed threshold for rotor angles as a mean to determine transient stability of the system.

1-3. A New Method to Incorporate Transient Stability Constraints

Optimal power flow (OPF) is a very important tool in power system planning and operation. Early research on OPF only takes static security constraints into account [25], [26], and the resulting dispatches may lead to transient instability under some critical or severe contingencies. To overcome this issue, the transient stability constrained optimal power flow (TSCOPF) was introduced in [27] and has become a new challenge in the recent years.

TSCOPF can be modeled as a large-scale nonlinear programming problem including the constraints of differential-algebraic equations (DAE). Solving a TSCOPF problem can be challenging due to (i) the differential-equation constraints in an optimization problem, (ii) the lack of a true analytical expression for transient stability constraint in OPF. The direct discretization of the differential equations was proposed in [29], and utilized in [31]-[39]. A functional transformation technique was proposed in [30] to handle differential equations by converting the infinite-dimensional TSCOPF into a finite-dimensional optimization problem. Unfortunately, even the current best TSCOPF solvers still suffer from the curse of dimensionality and unacceptable computational time, especially for large-scale power systems with multiple contingencies [37]. Furthermore, it has been

shown in [40] that the widely used fixed-threshold proxi for enforcing transient stability in TSCOPF can lead to both severe underestimated and overestimated assessments as well as degradations of the optimal solutions. To further improve the performance and usability of the discretization-based TSCOPF methods on large-scale practical power systems, it is crucial that the above issues must be addressed and corrected. In chapter 5, thse issues will be addressed and a new method to incorporate the transient stability constraints will be presented.

Chapter 2 Single Period SuperOPF

The SuperOPF problem is a super-set of the standard optimal power flow problem such as solved by MATPOWER [1, 2, 3]. The security of the dispatch is taken into account by including a copy of the system for each credible contingency, each with its own dispatch and probability-weighted cost of operation. This is accomplished by simply joining these copies to form one single large network with multiple "islands" and appropriately scaled generator costs. Additional linear constraints are added to restrict by a ramp rate limit the deviation of each generator's dispatch in each contingency from its corresponding base case dispatch. New variables are included, along with the inequalities that define their relationships to one another and to the dispatches, in order to impose additional costs. The overall structure of can be illustrated graphically as shown in Figure 2-1.

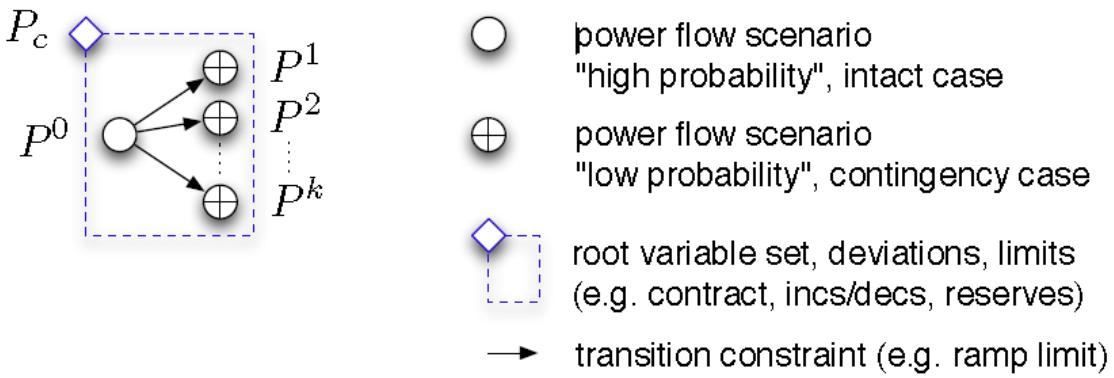

Figure 2-1: Graphical Representation of Co-optimization Structure

There are three types of additional variables added. First, for each generator *i* there is a variable representing an optimal energy contract, namely p_{ci}. This variable is used as a reference from which upward and downward deviations can be measured.

In fact, the second set of variables and p_{ik}^{-} represent the upward and downward deviations, respectively, of the dispatch of generator *i* in contingency *k* from the contract p_{ci}. These are sometimes refered to as incs and decs. The third set of variables r_{Pi}^{+} and r_{Pi}^{-} are simply the maximums of these deviations over all contingencies. In other words, r_{pi}^{+} is the maximum of p_{ik}^{+} over all *k*. These represent the reserve capacity needed in order to meet the full range of contingencies being considered. The relationships between these variables are illustrated in Figure 2-2.

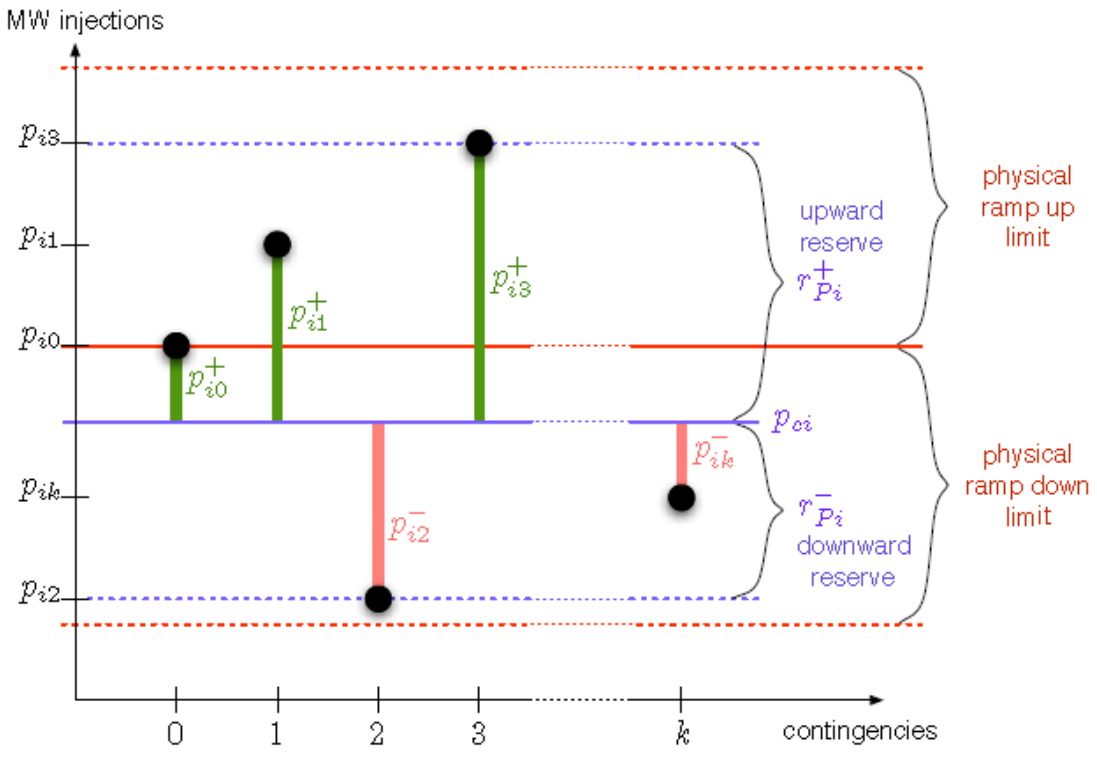

Figure 2-2: Contract, Incs/Decs and Reserve

2.1 Nomenclature

p_{ik}; q_{ik}	ith active and reactive injection in kth post-contingency state (k = 0 for base case).
$C_{Pi}(\cdot)$; $C_{Qi}(\cdot)$	Cost function for ith active and reactive injections.
p_{ci}, q_{ci}	Purchase amounts specified in the day-ahead contract for active and reactive power from the ith injection.
p_{ik}^{+} , q_{ik}^{+}	ith active and reactive upward deviations from contracted amount in k-th post-contingency state; k = 0 means realized deviation from contract with no contingencies.
$C_{Pi}^{+}(\cdot)$;$C_{Qi}^{+}(\cdot)$	Cost for incremental deviations from contract day-ahead quantity.
p_{ik}^{-}, q_{ik}^{-}	ith active and reactive downward deviations from contracted amount in kth post-contingency state.

$C_{Pi}^{-}(\cdot); C_{Qi}^{-}(\cdot)$	Cost for decremental deviations from contracted day-ahead quantity.
r_{Pi}^{+} , r_{Qi}^{+}	Upward active and reactive reserve amount provided by *i*th injection.
$C_{RPi}^{+}(\cdot); C_{RQi}^{+}(\cdot)$	Cost functions for upward reserve purchased from *i*th injection.
r_{Pi}^{-} , r_{Qi}^{-}	Downward active and reactive reserve amount provided by *i*th injection.
$C_{RPi}^{-}(\cdot); C_{RQi}^{-}(\cdot)$	Cost functions for downward reserve purchased from *i*th injection.
$(\Theta^k; V^k; P^k; Q^k)$	Voltage angles and magnitudes, active and reactive injections for power flow in *k*th post-contingency state (*k* = 0 means no contingency occured).
$g^k(\cdot)$	Nonlinear power flow equations in *k*th post-contingency state.
$h^k(\cdot)$	Transmission, voltage, generation and other limits in *k*th post-contingency state.
π_k	Probability of *k*th contingency (π_0 is the probability of no contingency).
n_g	Number of generators and dispatchable or curtailable loads initially available.
n_c	Number of contingencies considered.
G^k	Set of indices of generators present in the *k*th contingency.

Individual variables can be grouped in vectors, such as p_{ik} into P^k, and it will be consistent with the context.

2.2 Stage 1 - Day-Ahead Problem

The first stage or day-ahead problem is formulated as the following non-linear, constrained optimization problem.

$$\min_{\substack{\Theta, V, P, Q, \\ P^+, P^-, Q^+, Q^-, \\ P_c, Q_c, R_P, R_Q}} \quad f_P(P) + f_Q(Q) + f_{RP}(R_P) + f_{RQ}(R_Q) \tag{2.1}$$

The active power cost component is

$$f_P(P) = \sum_{k=0}^{n_c} \pi_k \sum_{i \in G^k} \left[C_{Pi}(p_{ik}) + C_{Pi}^+(p_{ik}^+) + C_{Pi}^-(p_{ik}^-) \right], \tag{2.2}$$

with three sub-components. Here, π_k is the probability of transition to the *k*th contingency from the day-ahead base case; $C_{Pi}(p_{ik})$ is the production cost or offer for the *i*th generator in the *k*th contingency; $C_{Pi}^+(p_{ik}^+)$ is an incremental cost, in addition to the production cost, on upward deviations from the day-ahead contracted quantity. Similarly, $C_{Pi}^-(p_{ik}^-)$ is an additional cost imposed on downward deviations from the day-ahead contract. These costs allow generators to signal a reluctance to vary their power output from the contracted day-ahead quantities. Likewise, the reactive power cost is

$$f_Q(Q) = \sum_{k=0}^{n_c} \pi_k \sum_{i \in G^k} \left[C_{Qi}(q_{ik}) + C_{Qi}^+(q_{ik}^+) + C_{Qi}^-(q_{ik}^-) \right], \tag{2.3}$$

the active reserve cost is

$$f_{RP}(R_P) = \sum_{i=1}^{n_g} [C_{RPi}^+(r_{Pi}^+) + C_{RPi}^-(r_{Pi}^-)], \tag{2.4}$$

and the reactive reserve cost is

$$f_{RQ}(R_Q) = \sum_{i=1}^{n_g} [C_{RQi}^+(r_{Qi}^+) + C_{RQi}^-(r_{Qi}^-)]. \tag{2.5}$$

Here, upward and downward reserves define a dispatch range relative to the day-ahead contracted quantities, (p_{ci}; q_{ci}).

All of this is subject to nonlinear active and reactive power flow constraints in the base case flow and all contingencies,

$$g_P^k(\theta^k, V^k, P^k, Q^k) = 0, \quad k = 0 \dots n_c, \tag{2.6}$$

$$g_Q^k(\theta^k, V^k, P^k, Q^k) = 0, \quad k = 0 \dots n_c, \tag{2.7}$$

transmission capacity, generation capability curve, voltage limit, dispatchable load power factor, and maximum angular separation constraints for all flows,

$$h^k(\theta^k, V^k, P^k, Q^k) \leq 0, \quad k = 0 \dots n_c. \tag{2.8}$$

These represent all of the standard AC OPF constraints implemented by MATPOWER.

In addition, there are new constraints that couple the base case and the post-contingency flows, defining the deviation variables and the reserve variables. The first set defines the ranges of the upward deviation and upward reserve variables and how they bound one another,

$$0 \leq p_{ik}^+ \leq r_{Pi}^+ \leq R_{Pi}^{\max+}, \qquad 0 \leq q_{ik}^+ \leq r_{Qi}^+ \leq R_{Qi}^{\max+}, \qquad \forall i, k. \tag{2.9}$$

The next set does the same for downward deviations and reserves,

$$0 \leq p_{ik}^- \leq r_{Pi}^- \leq R_{Pi}^{\max-}, \qquad 0 \leq q_{ik}^- \leq r_{Qi}^- \leq R_{Qi}^{\max-}, \qquad \forall i, k. \tag{2.10}$$

And the next one defines the relationship of the upward and downward deviations to the injections and contract,

$$p_{ik} - p_{ci} = p_{ik}^+ - p_{ik}^-, \qquad q_{ik} - q_{ci} = q_{ik}^+ - q_{ik}^-, \qquad \forall i, k. \tag{2.11}$$

The contracted quantities can also be limited by lower and upper bounds.

$$\begin{array}{l} p_{ci}^{\min} \leq p_{ci} \leq p_{ci}^{\max}, \quad \forall i \\ q_{ci}^{\min} \leq q_{ci} \leq q_{ci}^{\max}, \quad \forall i \end{array} \tag{2.12}$$

Then, the deviations from the base case (not from the contracted amount) are bounded by the physical ramp rate of each unit.

$$\begin{array}{l} -\Delta_{Pi}^{-} \leq p_{ik} - p_{i0} \leq \Delta_{Pi}^{+} \\ -\Delta_{Qi}^{-} \leq q_{ik} - q_{i0} \leq \Delta_{Qi}^{+} \end{array} \quad \forall i, \quad k = 1 \ldots n_c \tag{2.13}$$

Finally, these constraints allow imposing or relaxing an equality constraint between the contracted quantities and the base case dispatch quantities by choice of α

$$\begin{array}{l} -\alpha \leq p_{i0} - p_{ci} \leq \alpha \\ -\alpha \leq q_{i0} - q_{ci} \leq \alpha \end{array} \quad \forall i, \tag{2.14}$$

so that the contracted quantity can be specified to be equal to the base case dispatch if so desired.

In this formulation, for the bounds in (2.9) and (2.10) to be tight at the solution it is necessary that marginal costs on deviations and reserves (p_{ik}^{+}, p_{ik}^{-}, r_{Pi}^{+}, r_{Pi}^{-}, q_{ik}^{+}, q_{ik}^{-}, r_{Qi}^{+}, r_{Qi}^{-}) be positive. They can be allowed to be zero but that may require adjusting the bounds to be tight as a post-solution procedure that does not affect the cost. Negative marginal costs are not appropriate for this formulation.

The solution to the day-ahead problem yields optimal day-ahead contract quantities (P_c, R_P^{+} , R_P^{-}, Q_c, R_Q^{+} , R_Q^{-}) as well as generation ranges; for all considered scenarios, the *i*th generator's active output will lie in [p_{ci}- r_{Pi}^{-}, p_{ci}+ r_{Pi}^{+}], except perhaps in the scenario in which that unit is o_-line as a result of a contingency. The treatment of the reactive output is similar. The day-ahead planning then results in a contract for providing a nominal quantity p_{ci} at a price determined by the chosen auction institution and the marginal cost of energy at the generator's location, with the additional obligation to abide by any redispatch issued by the ISO in real time within the range [p_{ci}- r_{Pi}^{-}, p_{ci}+ r_{Pi}^{+}]. Such redispatch incurs the incremental costs, in addition to energy costs, computed as a function of amount of the deviation from the energy contract. This range of generation is reflected in the amounts of reserve r_{Pi}^{+} and r_{Pi}^{-} procured from the *i*th generator. A day-ahead settlement can be executed or the parties can wait until the real-time pricing and redispatch is performed the next day.

2.3 Stage 2 - Real-Time Adjustment of Dispatch

The problem of balancing and pricing the real-time market is now subject to the contract issued the previous day. Reserve quantities have already been determined and payed for. To compute any needed resdispatch the ISO has available a generation range, together with the original energy and incremental energy offers, and the current state of the network. Incremental amounts and costs are now determined relative to the p_{ci} agreed upon the previous day.

Security is still desirable, of course, and the dispatch should still consider the possibility of transitioning to other network configurations as a result of contingencies. At this point in time, however, the probabilities of occurence for contingencies have changed and in some cases, such as the specific realized demand, the uncertainty may no longer exist. The time viewpoint available to the planner now is not the same as the one available the previous day. There is more information. Either the system is "intact" and exhibits the configuration of the base case (with perhaps a somewhat different demand) or a contingency has happened and the system has undergone a transition.

2.3.1 Redispatching the Intact System

Assume that an intact system configuration is realized; that is, the configuration contemplated in the base case, possibly with a slightly different demand. While the transition restrictions needed to enforce a secure dispatch should still be included in the model, the probabilities of contingencies used for a pricing run of the model should be set to zero, i.e., the contingencies did not materialize. However, the formulation to follow could also be used for an hour-ahead or 10 minute-ahead redispatch, in which case some probabilities would not be zero.

The problem formulation for the second stage problem can be found by taking the first stage problem, treating the energy contracts and reserves as fixed parameters, and simplifying. This results in the following formulation.

$$\min_{\substack{\Theta, V, P, Q, \\ P^+, P^-, \\ Q^+, Q^-}} \sum_{k=0}^{n_c} \pi_k \sum_{i \in G^k} \left\{ \begin{array}{c} C_{Pi}(p_{ik}) + C_{Qi}(q_{ik}) \\ +C^+_{Pi}(p^+_{ik}) + C^+_{Qi}(q^+_{ik}) \\ +C^-_{Pi}(p^-_{ik}) + C^-_{Qi}(q^-_{ik}) \end{array} \right\} \tag{2.15}$$

subject to

$$g^k_P(\theta^k, V^k, P^k, Q^k) = 0, \quad k = 0 \ldots n_c, \tag{2.16}$$

$$g^k_Q(\theta^k, V^k, P^k, Q^k) = 0, \quad k = 0 \ldots n_c, \tag{2.17}$$

$$h^k(\theta^k, V^k, P^k, Q^k) \leq 0, \quad k = 0 \ldots n_c, \tag{2.18}$$

$$0 \leq p^+_{ik} \leq \hat{r}^+_{Pi}, \qquad 0 \leq q^+_{ik} \leq \hat{r}^+_{Qi}, \qquad \forall i, k, \tag{2.19}$$

$$0 \leq p^-_{ik} \leq \hat{r}^-_{Pi}, \qquad 0 \leq q^-_{ik} \leq \hat{r}^-_{Qi}, \qquad \forall i, k, \tag{2.20}$$

$$p_{ik} - \hat{p}_{ci} = p^+_{ik} - p^-_{ik}, \qquad q_{ik} - \hat{q}_{ci} = q^+_{ik} - q^-_{ik}, \qquad \forall i, k. \tag{2.21}$$

$$\begin{array}{l} -\Delta^-_{Pi} \leq p_{ik} - p_{i0} \leq \Delta^+_{Pi} \\ -\Delta^-_{Qi} \leq q_{ik} - q_{i0} \leq \Delta^+_{Qi} \end{array} \quad \forall i, \quad k = 1 \ldots n_c, \tag{2.22}$$

where ($\hat{P}_c, \hat{R}^+_P, \hat{R}^-_P, \hat{Q}_c, \hat{R}^+_Q, \hat{R}^-_Q$) are now fixed parameters, taken from the day-ahead solution. There is no need to enforce box (P_{min}, P_{max}, Q_{min}, Q_{max}) limits, since they are implicit in ($\hat{r}^+_{Pi}$, $\hat{r}^-_{Pi}$, $\hat{r}^+_{Qi}$, $\hat{r}^-_{Qi}$). However, it should be noted that for generators with trapezoidal feasible regions like those employed in MATPOWER, the upper and lower sloped linear constraints still need to be enforced (which MATPOWER does) and if binding, the corresponding shadow prices can be decomposed into equivalent μP_{max} and μP_{min} multipliers.

2.3.2 Redispatching in a Post-Contingency State

If the day-ahead base case no longer describes the current system configuration, possibly due to a contingency of some sort, transitions to the previously anticipated contingencies from the current state would represent what would have been an (N - 2)-type event the day ahead. While the transition to the present state should have been feasible thanks to the resources committed day-ahead, it is by no means clear that transitioning to yet

another contingency state from here will be feasible given the current set of contracted resources. Yet, it makes sense to try to run the problem (2.15)-(2.22), with the base case replaced by the present system state and a new set of (currently) credible contingencies, to see if it is still possible to redispatch the system securely and economically with the available resources. In extreme cases, it may not be feasible to consider any further contingencies in dispatching the currently available resources. In any case, a stage 1 problem, in which additional reserves are procured, may need to be solved for the next period in order to return to an acceptable level of security going forward.

Chapter 3: Multi-period SuperOPF

3.1 Introduction

Proper day-ahead scheduling should include consideration of inter-temporal constraints in adjacent hours. The most important class of these are the load-following ramp-up constraints; there should be enough ramp-up capability available to follow the morning peak, otherwise operation is simply not feasible. Two types of decisions affect preparedness for the morning peak: the type, number, capacity, location and ramp capability of the units that are online (as decided in the scheduling problem known as unit commitment), and the actual scheduling of the pool of units currently committed. These decisions must also take into account uncertain events such as falling wind output exactly as the system tries to follow the peaking load. Of course, ramp-down capability is also important in some cases. Additionally, some resources require planning across a time horizon due to constraints arising from technical or regulatory considerations. Pumped storage plants must obey the former category of constraints; other plants with regulated types of emissions (via caps/quotas or taxes) fall in the latter.

This section focuses solely on the amount of remediation that can be provided by proper scheduling of an a priori set of committed generators and dispatchable storage in light of possible violation of ramp-up capabilities when trying to meet load peaks, particularly if renewable sources happen to falter simultaneously. The formulation devised here will then be a fundamental part of the problem that includes the actual binary unit commitment decision variables.

On the day of the execution of the contract, closer to real time, with fixed contracts for reserve quantities, the uncertainty in wind, load and contingencies should diminish, and hour-ahead redispatches should be carried out using a receding-horizon strategy. The redispatch should consider a time horizon starting next hour, bound by both the present state of the system and by technical constraints spreading into future hours, not just the immediately subsequent hour. Updated information should be used for all uncertain quantities. Of course, the result of this optimization, in true receding-horizon fashion, is

only implemented starting next hour (though orders would emanate at $t = 0$ for the production setpoint to be reached at $t = 1$, so that generators start ramping towards it), and at that time the optimization is re-run for the hour starting one hour further into the future. It is also important to note that when t = 1 arrives, the operating point may be slightly different from that mandated at $t = 0$, due to contingencies, small load prediction errors, and small or large wind output forecast errors. The optimization run at $t = 1$ for obtaining the commanded dispatch for $t = 2$ must include the actual physical initial state of the system at $t = 1$.

It is important to realize that including the time dimension in the problem and modeling ramp constraints the way it is done here is again a compromise between the goals of attaining security, accurately representing a stochastic program and keeping problem size manageable. In particular, when we choose to enforce ramp limits from any root scenario at time t to any root scenario at time $t + 1$, we are covering for extreme variations that may be very rare in actuality, particularly if the scenarios are chosen to represent the geographically multivariate tails of the wind output distribution in addition to the most plausible scenarios. But worst-case scenario planning dictates this in accordance with secure operation philosophy. Furthermore, and this is fundamental, a scenario in an orthodox stochastic program with a time dimension involves a complete trajectory through the planning horizon, which we are not doing. We are more properly using an operating point envelope, rather than a collection of trajectories, for scenario planning.

Thus, it is important to understand that while the idealized day-ahead problem treated in the original optimal day-ahead contract formulation is close to a formal two stage stochastic programming problem because most of the uncertainty is relegated to the occurrence of contingencies, when we add the horizon planning (time) dimension we have to further depart from stochastic programming orthodoxy, which would require considering complete trajectories through time as one scenario and would also require the use of many trajectories to properly sample the full set of possible trajectories.

Transitioning from the base cases of several scenarios at time t to other base cases at time t+1 involves the idea that the actual transition could happen in many different ways, and each possible transition has a certain probability of occurrence, conditional on the actual realized scenario at time t. A simple model of this setting is based on a probability transition matrix that relates the vector of base case probabilities at time t to the vector of scenario probabilities at time $t + 1$.

Storage units require special treatment in the multiple-scenario case. Because energy storage limits must be respected in every realization, and this must be so even when considering such multiple scenarios through time, one modeling choice would be to include a single set of dispatch variables for storage units through all of the scenarios. This, of course, limits flexibility of dispatch in the face of wind or renewable variability. A somewhat different approach was taken that offers some added flexibility. Instead of using actual stored energy quantity variables for each of the scenarios (which would require keeping track of trajectories through time and a geometric quantity of variables and restrictions), lower bound and upper bound variables on the amount of stored energy are used. Thus, a lower bound on stored energy on the central path at the end of period t depends on the lower bound at time $t - 1$ and the worst case depletion in the base cases of the scenarios considered at time t.

Additionally, in case of a contingency, the use of stored energy in such a situation must also respect energy storage limits. A parameter α is provided to weight the fraction of the time slice that is spent in the base case operation and in contingent operation, as the final leftover energy after the contingency is dependent on that. Normally, $\alpha = 0$ and the full length of the slice is spent in contingent operation.

Storage units can have an initial stored energy quantity, and they could also have a leftover stored energy at the end of the horizon or at any other endpoint in the transition tree, such as in a contingency. This energy has a value and its expected value must be subtracted from the objective function. The price of stored energy is data for the problem.

3.2 Relation to Control Problem

The problem described in this section can be thought of as a multi-stage tracking control problem; the first set of decision variables or, equivalently, control inputs, being decided upon in a day-ahead manner, have an inherent input delay. If offers for the next day starting at 0:00 are received by 12:00, then this delay ranges from 12 hours to 35 hours. These decision variables simply prepare the system for meeting the load the next day, using a secure strategy with least expected cost, whatever the actual outcome is the next day. The horizon considered is an *N*-1-secure look-ahead horizon, meaning that only the high probability path in the forward time direction is considered, together with first-order branches from this high probability path arising due to credible contingencies. The high probability path itself may be modeled using several scenarios, not just a central one. Transitions from each of these base scenarios at time *t* to any of the scenarios at time *t*+1 are assumed to be conditional only on the realized scenario at time *t*. This is a strong assumption that is put in place to emphasize security.

The second stage decision inputs must be specified one hour ahead; the input delay is thus one hour. These inputs must take into account decisions incorporated in the previous day's contracts, as long as *N* -1 security is maintained. If not, then all bets are off and other procedures, to be considered out-of-ordinary operation, must be employed, such as out-of-market commitment or procurement of reserve. A receding horizon formulation must be used here too in order to properly take into account intertemporal restrictions that will affect next hour's operation.

There may be other stages with a finer time scale, but these could be very similar in their design to the hour-ahead market. However, from the point of view of the tracking control problem, in real-time there are automatic controls in place that adjust the _nest deviations. This does not occur without some amount of error; small frequency deviations that are the result of similarly small power imbalances do exist, and are the result of tracking errors. The automated controls use this error to counteract these finer imbalances.

3.3 Nomenclature

This section summarizes the nomenclature for this multi-period problem problem. Indexing becomes especially tricky, and in order to simplify the indexing notation, the index literals and their order are maintained wherever possible. Furthermore, are used, so the superindex *tijk* refers to time period *t*, generator *i* (or dispatchable load or storage unit *i*), base scenario *j* and contingency *k*. Typical sets of indices include J^t, the set of root cases *j* considered in the *t*-th stage; *T*, the set of indices *t* of stages, typically $\{1 \ldots. n_t\}$.

Symbol	**Meaning**
Δ	Length of scheduling time slice in hours, typically 1 hour.
t	Index over time periods.
T	Set of indices of time periods in planning horizon, typically $\{1 \ldots. n_t\}$.
j	Index over scenarios.
J^t	Set of indices of all scenarios considered at time *t*.
k	Index over post-contingency cases (*k* = 0 for base case, i.e. no contingency occured).
K^{tj}	Set of indices of contingencies considered in scenario *j* at time *t*.
i	Index over injections (generation units, storage units and dispatchable or curtailable loads).
I^t	Indices of all units (generators, storage and dispatchable or curtailable loads) available for dispatch in any contingency at time *t*.
I^{tjk}	Indices of all units available for dispatch in post-contingency state *k* of scenario *j* at time *t*.
p^{tijk}, q^{tijk}	Active/reactive injection for unit *i* in post-contingency state *k* of scenario *j* at time *t*.
$C_P^{ti}(\cdot)$	Cost function for active injection *i* at time *t*.

p_c^{ti}	Active power contract quantity for unit *i* at time *t*.
p_+^{tijk}, p_-^{tijk}	Upward/downward deviation from active power contract quantity for unit *i* in post-contingency state *k* of scenario *j* at time *t*.
$C_{P+}^{ti}(\cdot)$, $C_{P-}^{ti}(\cdot)$	Cost for upward/downward deviation from active power contract quantity for unit *i* at time *t*.
r_+^{ti}, r_-^{ti}	Upward/downward active contingency reserve quantity provided by unit *i* at time *t*.
$C_{R+}^{ti}(\cdot)$, $C_{R-}^{ti}(\cdot)$	Cost function for upward/downward contingency reserve purchased from unit *i* at time *t*.
δ_+^{ti}, δ_-^{ti}	Upward/downward load-following ramping reserves needed from unit *i* at time *t* for transition to time *t* + 1.
$C_{\delta+}^{ti}(\cdot)$, $C_{\delta-}^{ti}(\cdot)$	Cost of upward/downward load-following ramp reserve for unit *I* at time *t*.
$C_\delta^i(\cdot)$	Quadratic, symmetric ramping cost on the difference between the dispatches for unit *i* in adjacent periods.
θ^{tjk},V^{tjk},p^{tjk},q^{tjk}	Voltage angles and magnitudes, active and reactive injections for power flow in post-contingency state *k* of scenario *j* at time *t*.
$g^{tjk}(\cdot)$	Nonlinear AC power flow equations in post-contingency state *k* of scenario *j* at time *t*.
$h^{tjk}(\cdot)$	Transmission, voltage and other limits in post-contingency state *k* of scenario *j* at time *t*.
P_{min}^{tijk}, P_{max}^{tijk}	Limits on active injection for unit *i* in post-contingency state *k* of scenario *j* at time *t*.
Q_{min}^{tijk}, Q_{max}^{tijk}	Limits on reactive injection for unit *i* in post-contingency state *k* of scenario *j* at time *t*.

δ^i_{max+} , δ^i_{min-}	Upward/downward load-following ramping reserve limits for unit *i*.
Δ^i_+, Δ^i_-	Upward/downward physical ramping limits for unit *i* for transitions from base ($k = 0$) to contingency cases.
s^{ti}_+, s^{ti}_-	Upper/lower bounds on the energy stored in storage unit *i* at the end of period *t*. For $t = 0$ this is a fixed input parameter representing the bounds at the beginning of the first period.
s^{ti}_{max}, s^{ti}_{min}	Stored energy (in MWh) max/min limits for storage unit *i* at time *t*.
s^i_0	Initial stored energy (expected) in storage unit *i*.
S^{0i}_{max}, S^{0i}_{min}	Lower/upper bounds on initial stored energy (expected) in storage unit *i*.
$S^{m_t{}^i}_{max}$, $S^{n_t{}^i}_{min}$	Lower/upper bounds on target stored energy (expected) in storage unit *i* at end of final period n^t.
p^{tijk}_{sc} , p^{tijk}_{sd}	Charge/discharge power injections of storage unit *i* in post-contingency state *k* of scenario *j* at time *t*.
C_{s0}	Cost associated with starting out with a given level of stored energy s_0 at time $t = 0$.
C_s	Vector of prices for contributions to terminal storage[1] from charging or discharging in non-terminal states.
C_{sc0} , C_{sd0}	Vector of prices for contributions to terminal storage[1] from charging/discharging in terminal end-of-horizon base states.
C_{sck} , C_{sdk}	Vector of prices for contributions to terminal storage[1] from charging/discharging in terminal contingency states.

[1] That is, expected leftover stored energy in terminal states

C_{tc0} , C_{tsc} , C_{tcd} — Weighted price vectors summarizing contributions to the value of terminal storage[1] from initial storage/charging/discharging, derived from C_s, C_{sc0}, C_{sd0}, C_{sck}, C_{sdk} See (3.91){(3.94) for details.

η^i_{in} , η^i_{out} — Charging/discharging (or pumping/generating) efficiencies for storage unit *i*.

η^i_{loss} — Fraction of stored energy lost per hour by storage unit *i*.

ψ^{tjk} — Probability of contingency *k* in scenario *j* at time *t* (ψ^{tj0} is the probability of no contingency, i.e. the base case, for scenario *j* at time *t*).

α — For contingency cases, the fraction of the time slice that is spent in the base case before the contingency occurs ($\alpha = 0$ means the entire period is spent in the contingency).

ψ^{tjk}_α — Probability ψ^{tjk} of contingency *k* in scenario *j* at time *t* adjusted for α.

$$\psi^{tjk}_\alpha = \begin{cases} \psi^{tj0} + \alpha \sum_{\kappa \in K^{tj} \neq 0} \psi^{tj\kappa}, & k = 0 \\ (1-\alpha)\psi^{tjk}, & \forall k \in K^{tj} \neq 0 \end{cases} \quad (3.1)$$

γ^t — Probability of making it to period *t* without branching off the central path in a contingency in periods 1 … *t* - 1.

$$\gamma^t = \sum_{j \in J^{t-1}} \psi^{(t-1)j0} = \sum_{j \in J^t, k \in K^{tj}} \psi^{tjk} \quad (3.2)$$

$\phi^{tj_2j_1}$ — Probability of transitioning to scenario j_2 in period *t* given that we were at scenario j_1 in period *t* - 1.

$\zeta^{tj_2j_1}$ — Binary valued mask indicating whether transition to scenario j_2 in period *t* from scenario j_1 in period *t* - 1 should be included in load-following ramp requirements.

u^{ti}	Binary commitment state for unit *i* in period *t*, 1 if unit is on-line, 0 otherwise.
v^{ti} , w^{ti}	Binary startup and shutdown states for unit *i* in period *t*, 1 if unit has a startup/shutdown event in period *t*, 0 otherwise.
τ_i^+ , τ_i^-	Minimum up and down times for unit *i* in number of periods.
C_v^{ti} , C_w^{ti}	Startup and shutdown costs for unit *i* at time *t* in $ per startup/shutdown.

Individual variables can be grouped into vectors such as p^t for all active injections considered across all scenarios and contingencies at hour *t* and it will be consistent with the context. The subset referring to scenario *j* would be p^{tj}.

3.4 Formulation

The problem formulation can be expressed as a mixed-integer nonlinear optimization problem, where the optimization variable *x* is comprised of all the θ, V, p, q, p_c, p_+, p_-, r_+, r_-, δ_+, δ_-, p_{sc}, p_{sd}, s_0, s_+, s_-, u, v, and w variables. The last three are binary and the rest continuous. For simplicity, the formulation restricts the treatment of costs, deviations, ramping and reserves to consider only active power, but an extension to include reactive counterparts is straightforward.

Objective Function

The objective then is to

$$\min_x f(x) \tag{3.3}$$

where *f(x)* is comprised of six components.

$$\begin{aligned} f(x) = {} & f_p(p, p_+, p_-) + f_r(r_+, r_-) + f_\delta(p) \\ & + f_{\mathrm{lf}}(\delta_+, \delta_-) + f_s(s_0, p_{\mathrm{sc}}, p_{\mathrm{sd}}) + f_{\mathrm{uc}}(v, w) \end{aligned} \tag{3.4}$$

Each part is expressed in terms of the individual optimization variables as follows.

--- cost of active power dispatch and redispatch

$$f_p(p, p_+, p_-) = \sum_{t\in T}\sum_{j\in J^t}\sum_{k\in K^{tj}} \psi_\alpha^{tjk} \sum_{i\in I^{tjk}} \left[C_P^{ti}(p^{tijk}) + C_{P+}^{ti}(p_+^{tijk}) + C_{P-}^{ti}(p_-^{tijk})\right] \quad (3.5)$$

--- cost of contingency reserves

$$f_r(r_+, r_-) = \sum_{t\in T}\gamma^t \sum_{i\in I^t} \left[C_{R+}^{ti}(r_+^{ti}) + C_{R-}^{ti}(r_-^{ti})\right] \quad (3.6)$$

--- cost of load-following ramping (wear and tear)

$$f_\delta(p) = \sum_{t\in T}\gamma^t \sum_{\substack{j_1\in J^{t-1}\\ j_2\in J^t}} \phi^{tj_2j_1} \sum_{i\in I^{tj_20}} C_\delta^i(p^{tij_20} - p^{(t-1)ij_10}) \quad (3.7)$$

--- cost of load-following ramp reserves

$$f_{\mathrm{lf}}(\delta_+, \delta_-) = \sum_{t\in T}\gamma^t \sum_{i\in I^t} \left[C_{\delta+}^{ti}(\delta_+^{ti}) + C_{\delta-}^{ti}(\delta_-^{ti})\right] \quad (3.8)$$

--- cost of initial stored energy and value (since it is negative) of expected leftover stored energy in terminal states

$$f_s(s_0, p_{\mathrm{sc}}, p_{\mathrm{sd}}) = C_{s0}^\top s_0 - (C_{\mathrm{ts}0}^\top s_0 + C_{\mathrm{tsc}}^\top p_{\mathrm{sc}} + C_{\mathrm{tsd}}^\top p_{\mathrm{sd}}) \quad (3.9)$$

--- startup and shutdown costs

$$f_{\mathrm{uc}}(v, w) = \sum_{t\in T}\gamma^t \sum_{i\in I^t} (C_v^{ti} v^{ti} + C_w^{ti} w^{ti}) \quad (3.10)$$

This minimization is subject to the following constraints, for all $t \in T$, all $j \in J^t$, all $k \in K^{tj}$, and all $i \in I^{tjk}$:

Standard OPF Constraints

--- nonlinear AC power balance equations

$$g^{tjk}(\theta^{tjk}, V^{tjk}, p^{tjk}, q^{tjk}) = 0 \quad (3.11)$$

--- nonlinear transmission flow limits, voltage limits, any other OPF inequality constraints

$$h^{tjk}(\theta^{tjk}, V^{tjk}, p^{tjk}, q^{tjk}) \leq 0 \tag{3.12}$$

Contingency Constraints

--- reserve, redispatch and contract variables

$$0 \leq p_{+}^{tijk} \leq r_{+}^{ti} \leq R_{\max+}^{ti} \tag{3.13}$$
$$0 \leq p_{-}^{tijk} \leq r_{-}^{ti} \leq R_{\max-}^{ti} \tag{3.14}$$
$$p^{tijk} - p_c^{ti} = p_{+}^{tijk} - p_{-}^{tijk} \tag{3.15}$$

--- ramping limits on transitions from base to contingency cases

$$-\Delta_{-}^{i} \leq p^{tijk} - p^{tij0} \leq \Delta_{+}^{i}, \quad k \neq 0 \tag{3.16}$$

Intertemporal Constraints

The first of the constraints to spread intertemporally are the load-following ramp constraints, including ramping from a known dispatch at $t = 0$ into the first period.

--- load-following ramping limits and reserves

$$0 \leq \delta_{+}^{ti} \leq \delta_{\max+}^{ti} \tag{3.17}$$
$$0 \leq \delta_{-}^{ti} \leq \delta_{\max-}^{ti} \tag{3.18}$$

for all $\{t \in T, i \in I^{tjk}, j_1 \in J^{t-1}, j_2 \in J^t \mid \zeta^{tj_2j_1} = 1\}$:

$$p^{tij_20} - p^{(t-1)ij_10} \leq \delta_{+}^{(t-1)i} \tag{3.19}$$
$$p^{(t-1)ij_10} - p^{tij_20} \leq \delta_{-}^{(t-1)i} \tag{3.20}$$

--- storage constraints

$$p^{tijk} = p_{\text{sc}}^{tijk} + p_{\text{sd}}^{tijk} \tag{3.21}$$
$$p_{\text{sc}}^{tijk} \leq 0 \tag{3.22}$$
$$p_{\text{sd}}^{tijk} \geq 0 \tag{3.23}$$
$$s_{-}^{ti} \geq S_{\text{min}}^{ti} \tag{3.24}$$
$$s_{+}^{ti} \leq S_{\text{max}}^{ti} \tag{3.25}$$

If the net increase in stored energy due to charging or discharging for unit *i* in state *tjk* is defined as

$$s_{\Delta}^{tijk} \equiv -\Delta(\eta_{\text{in}}^{i} p_{\text{sc}}^{tijk} + \frac{1}{\eta_{\text{out}}^{i}} p_{\text{sd}}^{tijk}), \tag{3.26}$$

then the bound and injection variables are constrained as follows.

$$s_{-}^{ti} \leq \beta_1^i s_{-}^{(t-1)i} + \beta_2^i s_{\Delta}^{tij0} \tag{3.27}$$
$$s_{+}^{ti} \geq \beta_1^i s_{+}^{(t-1)i} + \beta_2^i s_{\Delta}^{tij0} \tag{3.28}$$
$$S_{\text{min}}^{ti} \leq \beta_5^i s_{-}^{(t-1)i} + \beta_4^i s_{\Delta}^{tij0} + \beta_3^i s_{\Delta}^{tijk}, \quad k \neq 0 \tag{3.29}$$
$$S_{\text{max}}^{ti} \geq \beta_5^i s_{+}^{(t-1)i} + \beta_4^i s_{\Delta}^{tij0} + \beta_3^i s_{\Delta}^{tijk}, \quad k \neq 0 \tag{3.30}$$

where β_1^i, β_2^i, β_3^i, β_4^i, and β_5^i are defined in (3.48) and (3.56)–(3.58).

--- additional optional storage constraints

Option 1 is to constrain the expected final stored energy in each unit at the end of the horizon[2] to equal some target value or lie in some target range.

$$S_{\text{min}}^{n_t i} \leq s_F^{n_t i} \leq S_{\text{max}}^{n_t i} \tag{3.31}$$

Option 2 is to constrain the expected final stored energy at the end of the horizon[2] to equal the initial stored energy.

2See (3.80) in the next section for details on how $s_F^{n_t i}$ is computed as a linear function of *x*.

$$s_F^{n_t i} = s_0^i \tag{3.32}$$
$$S_{\min}^{0i} \leq s_0^i \leq S_{\max}^{0i} \tag{3.33}$$

When using this option S_0^i is an optimization variable that can take on any value between its bounds. When not using this option, it is simply a fixed parameter.

Unit Commitment

--- injection limits and commitments

$$u^{ti} P_{\min}^{tijk} \leq p^{tijk} \leq u^{ti} P_{\max}^{tijk} \tag{3.34}$$
$$u^{ti} Q_{\min}^{tijk} \leq q^{tijk} \leq u^{ti} Q_{\max}^{tijk} \tag{3.35}$$

--- startup and shutdown events

$$u^{ti} - u^{(t-1)i} = v^{ti} - w^{ti} \tag{3.36}$$

--- minimum up and down times

$$\sum_{y=t-\tau_i^+}^{t} v^{yi} \leq u^{ti} \tag{3.37}$$

$$\sum_{y=t-\tau_i^-}^{t} w^{yi} \leq 1 - u^{ti} \tag{3.38}$$

--- integrality constraints

$$u^{ti} \in \{0,1\}, v^{ti} \in \{0,1\}, w^{ti} \in \{0,1\} \tag{3.39}$$

This formulation for storage accommodates several types of resources. A traditional pumped-storage unit fits the model perfectly, as does a battery that does not have to go through specific charge-discharge curves that span many time slices (even if the batteries do have to go through such curves, a farm of such batteries may mimic an overall battery with more dispatching flexibility). A combined ice storage plus air conditioning facility can also be modeled. Even dispatchable loads with an energy consumption quota over a given horizon can be specified by manipulation of (S_{min}^{ti} , S_{max}^{ti}).

The assumptions regarding the probabilistic weighting of each term in the cost function are described now. We start with probability 1 in some initial state at $t = 0$; active dispatches and storage unit states are assumed known. From this initial state, transitions, each with some known probability, are possible to any of the scenarios considered for period $t = 1$. Thus, for period $t = 1$, the sum of the probabilities assigned to each of the flows adds up to 1. Now, consider the transition into $t = 2$. This transition is only possible provided that the system did not branch off into any contingency at time t = 1, that is, the realized state is the base case of one of the scenarios considered for $t = 1$. However, the sum of the probabilities of the considered base cases for $t = 1$ is less than 1 provided that at least one contingency has a nonzero probability of occurrence (the normal assumption). Thus, the probability of actually making it to $t = 2$ in the considered graph is equal to the sum of the probabilities of the base cases at $t = 1$, and is less than 1 except for $t = 1$:

$$\gamma^t = \sum_j \psi^{(t-1)j0} = \sum_{j,k} \psi^{tjk} < 1, \quad t > 1 \tag{3.40}$$

While the fact that the probabilities in future periods do not sum to one may seem odd in a non-stochastic scheme, this is the result of the fact that, in an $N - 1$ contingency fashion, we chose to know nothing about the cost incurred after branching off in a contingency because that would involve exploration of the geometric possibilities of resuming normal operation afterwards. This implies, for the branches that have been trimmed, the existence of an unknown cost with respect to the decision variables. Since we do not have any information about the relationship of this unknown cost to our decisions, we explicitly ignore its impact by excluding it from the optimization.

Transition probabilities are governed by a known probability transition matrix at each time step:

$$\begin{bmatrix} \sum_k \psi^{t1k} \\ \sum_k \psi^{t2k} \\ \vdots \\ \sum_k \psi^{tn_{Jt}k} \end{bmatrix} = \Phi^t \begin{bmatrix} \psi^{(t-1)10} \\ \psi^{(t-1)20} \\ \vdots \\ \psi^{(t-1)n_{Jt-1}0} \end{bmatrix} \tag{3.41}$$

where n_{Jt} is the number of scenarios considered at period *t*. Here, the columns of Φ^t sum to 1, and in fact its coefficients are used to weight the wear and tear costs included in the formulation:

$$\Phi^t = \begin{bmatrix} \phi^{t11} & \phi^{t12} & \cdots & \phi^{t1n_{Jt-1}} \\ \phi^{t21} & \phi^{t22} & \cdots & \phi^{t2n_{Jt-1}} \\ \vdots & \vdots & \ddots & \vdots \\ \phi^{tn_{Jt}1} & \phi^{tn_{Jt}2} & \cdots & \phi^{tn_{Jt}n_{Jt-1}} \end{bmatrix} \tag{3.42}$$

Finally, it is useful to include general linear production constraints that can be imposed over specific sets of generator, time slice, scenario and contingency tetrads (*t*; *i*; *j*; *k*) such as C^l = {(1, 3, 1, 0), (2, 3, 1, 0) … (n_t, 3, 1, 0)}, and which take the form

$$b_L^l \leq \sum_{(t,i,j,k)\in C^l} c^{tijkl} p^{tijk} \leq b_R^l, \tag{3.43}$$

each of which is completely defined by the index set C^l, a linear coefficient vector c^l and corresponding left and right hand sides b_L^l and b_R^l. More generally, with $x = (\theta, V, p, q, p_c, p_+, p_-, r_+, r_-, \delta_+, \delta_-, s_+, s_-)$, these constraints can be written as

$$b_L \leq \sum_{t\in T} M^t x^t \leq b_R \tag{3.44}$$

which is of course a block-column representation of

$$b_L \leq Mx \leq b_R, \tag{3.45}$$

but we adopt the former because it is appropriate for explaining decomposition techniques. In Figure 3-1, a graphical representation of the problem is depicted.

3.5 Value of Residual Storage

The details of the fifth term $f_5(\cdot)$ of the objective function (3.4) are presented in this section, specifically the last three terms of (3.9) related to the expected residual value

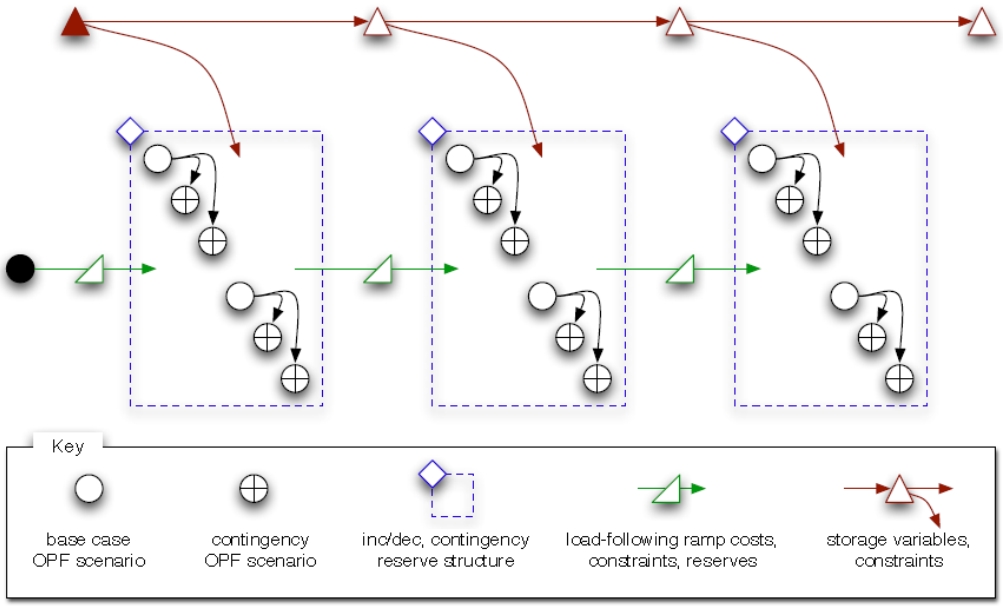

Figure 3-1: Overall Problem Structure

of stored energy in terminal states. First, for each storage resource *i*, this requires an efficient way to compute the expected amount of stored energy at the beginning and end of each period *t* for each scenario *j*. We will denote these by the n_{Jt} x 1 vectors S_I^{ti} and S_F^{ti}, respectively, where n_{Jt} is the number of scenarios in period *t*.

The stored energy s_F^{tij0} in unit *i* at the end of period *t* in base state *j* can be computed deterministically from the stored energy at the beginning s_I^{tij0} and the injections in that state, where the losses are assumed to be proportional to the average stored energy during the period. Using the definition in (3.26), this relationship can be expressed as follows

$$s_F^{tij0} = s_I^{tij0} + s_\Delta^{tij0} - \Delta\eta_{\text{loss}}^i \frac{s_I^{tij0} + s_F^{tij0}}{2} \tag{3.46}$$

$$= \beta_1^i s_I^{tij0} + \beta_2^i s_\Delta^{tij0}, \tag{3.47}$$

where

$$\beta_1^i \equiv \frac{1-\Delta\frac{\eta_{\text{loss}}^i}{2}}{1+\Delta\frac{\eta_{\text{loss}}^i}{2}}, \quad \beta_2^i \equiv \frac{1}{1+\Delta\frac{\eta_{\text{loss}}^i}{2}}. \tag{3.48}$$

For a period where a contingency occurs at a fraction α of the way through the period, the losses are more tricky to compute. Let us call the expected stored energy at the moment the contingency occurs s_α^{tijk}, expressed as

$$s_\alpha^{tijk} = s_I^{tijk} + \alpha(s_F^{tij0} - s_I^{tijk}). \tag{3.49}$$

Then the losses are equal to

$$s_{\text{loss}}^{tijk} = \Delta\eta_{\text{loss}}^i \left[\alpha\frac{s_I^{tijk}+s_\alpha^{tijk}}{2} + (1-\alpha)\frac{s_\alpha^{tijk}+s_F^{tijk}}{2}\right] \tag{3.50}$$

$$= \Delta\eta_{\text{loss}}^i \left[\alpha\frac{s_I^{tij0}+s_F^{tij0}}{2} + (1-\alpha)\frac{s_I^{tijk}+s_F^{tijk}}{2}\right] \tag{3.51}$$

where (3.51) follows directly from (3.49) and (3.50), keeping in mind that $s_I^{tijk} = s_I^{tij0}$.

In this case, the stored energy in unit *i* at the end of period *t* in state *jk* can be computed deterministically from the stored energy at the beginning and the injections in states *j*0 and *jk* as follows.

$$s_F^{tijk} = s_I^{tijk} + \alpha s_\Delta^{tij0} + (1-\alpha)s_\Delta^{tijk} - s_{\text{loss}}^{tijk} \tag{3.52}$$

$$= \alpha\left[s_I^{tij0} + s_\Delta^{tij0} - \Delta\eta_{\text{loss}}^i\frac{s_I^{tij0}+s_F^{tij0}}{2}\right]$$

$$+ (1-\alpha)\left[s_I^{tijk} + s_\Delta^{tijk} - \Delta\eta_{\text{loss}}^i\frac{s_I^{tijk}+s_F^{tijk}}{2}\right] \tag{3.53}$$

$$= \alpha\left[\beta_1^i s_I^{tij0} + \beta_2^i s_\Delta^{tij0}\right] + (1-\alpha)\left[s_I^{tijk} + s_\Delta^{tijk} - \Delta\eta_{\text{loss}}^i\frac{s_I^{tijk}+s_F^{tijk}}{2}\right] \tag{3.54}$$

$$= \beta_5^i s_I^{tijk} + \beta_4^i s_\Delta^{tij0} + \beta_3^i s_\Delta^{tijk} \tag{3.55}$$

where

$$\begin{aligned}\beta_3^i &\equiv \left(\frac{1}{1-\alpha} + \Delta\frac{\eta_{\text{loss}}^i}{2}\right)^{-1} \\ &= \frac{1-\alpha}{1+(1-\alpha)\Delta\frac{\eta_{\text{loss}}^i}{2}} \qquad (3.56)\\ \beta_4^i &\equiv \frac{\alpha}{1-\alpha}\beta_2^i\beta_3^i \\ &= \frac{\alpha}{(1+\Delta\frac{\eta_{\text{loss}}^i}{2})(1+(1-\alpha)\Delta\frac{\eta_{\text{loss}}^i}{2})} \qquad (3.57)\end{aligned}$$

$$\begin{aligned}\beta_5^i &\equiv \frac{\beta_1^i}{\beta_2^i}(\beta_3^i + \beta_4^i) \\ &= \left(1 - \Delta\frac{\eta_{\text{loss}}^i}{2}\right)\frac{\alpha + (1-\alpha)(1+\Delta\frac{\eta_{\text{loss}}^i}{2})}{(1+\Delta\frac{\eta_{\text{loss}}^i}{2})(1+(1-\alpha)\Delta\frac{\eta_{\text{loss}}^i}{2})} \qquad (3.58)\end{aligned}$$

Let G_k^{ti} and H_k^{ti} be matrices containing appropriately placed efficiencies relating the charging and discharging injections, respectively, in state *jk* of storage unit *i* in period *t* to the corresponding change in stored energy from the beginning to the end of the period. Specifically, the elements g_{jl}^{ti} and h_{jl}^{ti} in row *j* and column *l* of G_k^{ti} and H_k^{ti} are set as follows

$$g_{jl}^{ti} = \begin{cases} -\Delta\eta_{\text{in}}^i, & \text{where column } l \text{ corresponds to } p_{\text{sc}}^{tijk} \\ 0, & \text{otherwise} \end{cases} \qquad (3.59)$$

$$h_{jl}^{ti} = \begin{cases} -\Delta\dfrac{1}{\eta_{\text{out}}^i}, & \text{where column } l \text{ corresponds to } p_{\text{sd}}^{tijk} \\ 0, & \text{otherwise} \end{cases} \qquad (3.60)$$

The reason for keeping G_k^{ti} and H_k^{ti} separate is to make it possible to use different prices to represent the gain in value from increasing the amount of residual storage and the loss in value from reducing the amount of residual storage. The need to use different prices to value charging and discharging is supported by the intuition that stored energy should not be used in a given terminal state if there is a better time to use it (expect a higher price on the horizon), neither should we be storing additional energy in a given terminal state if there is a better time to store it (expect a lower price on the horizon).

Using these matrices, (3.47) can be expressed for the vector S_F^{ti} as a deterministic function of S_I^{ti} and the injections as

$$S_F^{ti} = \beta_1^i S_I^{ti} + \beta_2^i (G_0^{ti} + H_0^{ti}) x \tag{3.61}$$

On the other hand, the expected stored energy in each scenario at the beginning of period *t* depends on the corresponding values at the end of period *t* - 1 and the transition probabilities. Let σ^t equal the vector of probabilities of each of the base scenarios at the end of period *t* - 1, conditional on arriving at the end of that period without the occurence of a contingency.

$$\sigma^t \equiv \frac{1}{\gamma^t} \psi^{(t-1)J0} = \frac{1}{\gamma^t} \begin{bmatrix} \psi^{(t-1)10} \\ \psi^{(t-1)20} \\ \vdots \\ \psi^{(t-1)n_{Jt-1}0} \end{bmatrix} \tag{3.62}$$

If we also let $[a]$ denote a diagonal matrix with the vector a on the main diagonal, then the relationship between S_I^{ti} and $S_F^{(t-1)i}$ can be expressed as

$$\left[\Phi^t \sigma^t\right] S_I^{ti} = \Phi^t \left[\sigma^t\right] S_F^{(t-1)i}. \tag{3.63}$$

In other words,

$$S_I^{ti} = D^{ti} S_F^{(t-1)i} \tag{3.64}$$

where

$$D^{ti} \equiv \begin{cases} \mathbf{1}_{n_{Jt} \times 1}, & t = 1 \\ \left[\Phi^t \sigma^t\right]^{-1} \Phi^t \left[\sigma^t\right], & t \neq 1. \end{cases} \tag{3.65}$$

Stacking the vectors S_I^{ti} and S_F^{ti} for all storage units (*i* from 1 to n_s) allows the relationships above to be expressed in terms of matrices formed by stacking the D^{ti} along the diagonals and the G_k^{ti} and H_k^{ti} vertically.

$$D^t = \begin{bmatrix} D^{t1} & 0 & \cdots & 0 \\ 0 & D^{t2} & \cdots & 0 \\ \vdots & \vdots & \ddots & \vdots \\ 0 & 0 & \cdots & D^{tn_s} \end{bmatrix}, G_k^t = \begin{bmatrix} G_k^{t1} \\ G_k^{t2} \\ \vdots \\ G_k^{tn_s} \end{bmatrix}, H_k^t = \begin{bmatrix} H_k^{t1} \\ H_k^{t2} \\ \vdots \\ H_k^{tn_s} \end{bmatrix} \tag{3.66}$$

Similarly, scalars β_n^i are converted to diagonal matrices $B_n^{ti} \equiv \beta_n^i \cdot I_{n_{Jt} \times n_{Jt}}$ and stacked to form

$$B_n^t = \begin{bmatrix} B_n^{t1} & 0 & \cdots & 0 \\ 0 & B_n^{t2} & \cdots & 0 \\ \vdots & \vdots & \ddots & \vdots \\ 0 & 0 & \cdots & B_n^{tn_s} \end{bmatrix}. \tag{3.67}$$

The full expression for all storage units in all scenarios in period *t* can then be expressed as follows.

$$S_I^t = D^t S_F^{(t-1)} \tag{3.68}$$
$$S_F^t = B_1^t S_I^t + B_2^t (G_0^t + H_0^t) x \tag{3.69}$$

The relationships in (3.68) and (3.69) imply that the expected stored energy at any point in the planning horizon can be expressed in the following form as a linear function of the expected initial stored energy s_0 and the active power injections in *x*, specifically the injections of the storage units.

$$S_I^t = L_I^t s_0 + (M_g^t + M_h^t) x \tag{3.70}$$
$$S_F^t = L_F^t s_0 + (N_g^t + N_h^t) x \tag{3.71}$$

The following recursive expressions can be used for computing L_I^t , L_F^t, M_g^t, M_h^t , N_g^t and N_h^t

$$L_I^t = D^t L_F^{(t-1)} = D^t B_1^{(t-1)} L_I^{(t-1)} \tag{3.72}$$
$$L_F^t = B_1^t L_I^t = B_1^t D^t L_F^{(t-1)} \tag{3.73}$$
$$M_g^t = D^t N_g^{(t-1)} \tag{3.74}$$
$$M_h^t = D^t N_h^{(t-1)} \tag{3.75}$$
$$N_g^t = B_1^t M_g^t + B_2^t G_0^t \tag{3.76}$$
$$N_h^t = B_1^t M_h^t + B_2^t H_0^t, \tag{3.77}$$

where $L_I^1 = D^1$ and $M_g^1 = M_h^1 = 0$.

If the rows of each of these vectors and matrices are sorted and partitioned by scenario (as opposed to by storage unit), we can denote the resulting *j*-th components, whose *i*-th row corresponds to storage unit *i*, with a bar, for example $\bar{S}_F^{tj}$, $\bar{S}_I^{tj}$, $\bar{G}_k^{tj}$, $\bar{H}_k^{tj}$, $\bar{L}_I^{tj}$, $\bar{L}_F^{tj}$, $\bar{M}_g^{tj}$, $\bar{M}_h^{tj}$, $\bar{N}_g^{tj}$ and $\bar{N}_h^{tj}$. It should be noted that for the *B* matrices, the corresponding $\bar{B}_n^{tj}$ is just the diagonal matrix [β_n], with the individual β_n^i on the diagonal. Using this notation, the expected residual stored energy for all units in a base scenario *j* at the end of the last period n_t of the horizon, the vector $\bar{S}_F^{n_t j}$ can be written as a function of these matrices

$$\begin{aligned}\bar{S}_F^{n_t j} &= [\beta_1]\bar{S}_I^{n_t j} + [\beta_2](\bar{G}_0^{n_t j} + \bar{H}_0^{n_t j})x \\ &= [\beta_1]\left(\bar{L}_I^{n_t j} s_0 + (\bar{M}_g^{n_t j} + \bar{M}_h^{n_t j})x\right) + [\beta_2](\bar{G}_0^{n_t j} + \bar{H}_0^{n_t j})x \\ &= [\beta_1]\bar{L}_I^{n_t j} s_0 + \left([\beta_1]\bar{M}_g^{n_t j} + [\beta_2]\bar{G}_0^{n_t j} + [\beta_1]\bar{M}_h^{n_t j} + [\beta_2]\bar{H}_0^{n_t j}\right) x. \end{aligned} \tag{3.78}$$

Likewise, the expected residual stored energy at the end of period *t* for any scenario *j* and contingency *k* is expressed as follows,

$$\begin{aligned}\bar{S}_F^{tjk} &= [\beta_5]\bar{S}_I^{tj} + [\beta_4]\bar{S}_\Delta^{tj0} + [\beta_3]\bar{S}_\Delta^{tjk} \\ &= [\beta_5]\bar{S}_I^{tj} + \left([\beta_4](\bar{G}_0^{tj} + \bar{H}_0^{tj}) + [\beta_3](\bar{G}_k^{tj} + \bar{H}_k^{tj})\right) x \\ &= [\beta_5]\left(\bar{L}_I^{tj} s_0 + (\bar{M}_g^{tj} + \bar{M}_h^{tj})x\right) + \left([\beta_4](\bar{G}_0^{tj} + \bar{H}_0^{tj}) + [\beta_3](\bar{G}_k^{tj} + \bar{H}_k^{tj})\right) x \\ &= [\beta_5]\bar{L}_I^{tj} s_0 + \left([\beta_5]\bar{M}_g^{tj} + [\beta_4]\bar{G}_0^{tj} + [\beta_3]\bar{G}_k^{tj}\right. \\ &\qquad \left. + [\beta_5]\bar{M}_h^{tj} + [\beta_4]\bar{H}_0^{tj} + [\beta_3]\bar{H}_k^{tj}\right) x. \end{aligned} \tag{3.79}$$

The overall expected quantity of stored energy across all non-contingency states at the end of the horizon is given by

$$s_F^{n_t} = \frac{1}{\gamma^{(n_t+1)}} \sum_{j \in J^{n_t}} \psi^{n_t j 0} \bar{S}_F^{n_t j} \tag{3.80}$$

where $\gamma^{(n_t+1)} = \sum_j \psi^{n_t j 0}$. This expression can be used in constraints, such as (3.31) or (3.32) or in constructing terms of the objective function.

Finally, we return to the value, call it $v_s(x)$, of the expected stored energy leftover in terminal states, expressed in the last three terms of f_s in (3.9).

$$v_S(x) = C_{\text{ts0}}^{\mathsf{T}} s_0 + C_{\text{tsc}}^{\mathsf{T}} p_{\text{sc}} + C_{\text{tsd}}^{\mathsf{T}} p_{\text{sd}} \tag{3.81}$$

If we were to use a single price for each storage unit *i* to value all contributions to that expected leftover energy, regardless of the state in which they occur, then the value $v_s(x)$ would be that price times a simple probability-weighted sum of the energy in each state, modified by the output efficiency. To be more precise, the price relates to the value of each MW of *recoverable* energy[3] as opposed to *stored* energy.

$$v_S(x) = C_{\text{s}}^{\mathsf{T}}[\eta_{\text{out}}] \left(\sum_{j \in J^{n_t}} \psi^{n_t j 0} \bar{S}_F^{n_t j} + \sum_{t \in T} \sum_{j \in J^t} \sum_{k \in K^{tj} \neq 0} \psi^{tjk} \bar{S}_F^{tjk} \right) \tag{3.82}$$

However, it may be useful to classify the system states into three categories: terminal contingency states, terminal end-of-horizon base states, and non-terminal states (base states preceding the last period). This allows for the possibility of valuing differently the contributions made to the expected terminal stored energy in each of these categories of states. It may also be useful to differentiate between the value gained by increasing the expected terminal stored energy and the value lost by decreasing it.

Table 3-1: Five Price Model

price	applies to contributions from ...
C_s	charging and discharging in non-terminal states
C_{sc0}	charging in terminal end-of-horizon base states
C_{sd0}	discharging in terminal end-of-horizon base states
$C_{\text{sc}k}$	charging in terminal contingency states
$C_{\text{sd}k}$	discharging in terminal contingency states

[3] It is not the amount of energy stored that is of interest, but rather the amount which can be recovered after output efficiency losses η_{out}^i.

This leads to the current design based on the five price model summarized in Table 3-1. Expressing (3.82) in terms of (3.78) and (3.79), splitting up the terms and applying different prices to the five different types of contributions to the expected terminal storage quantities, yields the following.

$$v_S(x) = C_s^{\mathsf{T}}[\eta_{\text{out}}](A_1 s_0 + A_2 x + A_3 x) + C_{\text{sc}0}^{\mathsf{T}}[\eta_{\text{out}}]A_4 x + C_{\text{sd}0}^{\mathsf{T}}[\eta_{\text{out}}]A_5 x + C_{\text{sc}k}^{\mathsf{T}}[\eta_{\text{out}}]A_6 x + C_{\text{sd}k}^{\mathsf{T}}[\eta_{\text{out}}]A_7 x \tag{3.83}$$

where

$$A_1 = \sum_{j\in J^{n_t}} \psi^{tj0}[\beta_1]\bar{L}_I^{n_t j} + \sum_{t\in T}\sum_{j\in J^t}\left(\sum_{k\in K^{tj}\neq 0}\psi^{tjk}\right)[\beta_5]\bar{L}_I^{tj} \tag{3.84}$$

$$A_2 = \sum_{j\in J^{n_t}} \psi^{tj0}[\beta_1]\bar{M}_g^{n_t j} + \sum_{t\in T}\sum_{j\in J^t}\left(\sum_{k\in K^{tj}\neq 0}\psi^{tjk}\right)\left([\beta_5]\bar{M}_g^{tj} + [\beta_4]\bar{G}_0^{tj}\right) \tag{3.85}$$

$$A_3 = \sum_{j\in J^{n_t}} \psi^{tj0}[\beta_1]\bar{M}_h^{n_t j} + \sum_{t\in T}\sum_{j\in J^t}\left(\sum_{k\in K^{tj}\neq 0}\psi^{tjk}\right)\left([\beta_5]\bar{M}_h^{tj} + [\beta_4]\bar{H}_0^{tj}\right) \tag{3.86}$$

$$A_4 = \sum_{j\in J^{n_t}} \psi^{tj0}[\beta_2]\bar{G}_0^{n_t j} \tag{3.87}$$

$$A_5 = \sum_{j\in J^{n_t}} \psi^{tj0}[\beta_2]\bar{H}_0^{n_t j} \tag{3.88}$$

$$A_6 = \sum_{t\in T}\sum_{j\in J^t}\sum_{k\in K^{tj}\neq 0}\psi^{tjk}[\beta_3]\bar{G}_k^{tj} \tag{3.89}$$

$$A_7 = \sum_{t\in T}\sum_{j\in J^t}\sum_{k\in K^{tj}\neq 0}\psi^{tjk}[\beta_3]\bar{H}_k^{tj} \tag{3.90}$$

If we use $\bar{A}_n$ to represent the version of A_n with all columns removed except for those corresponding to the relevant charging and discharging injections (p_{sc} for n = 2, 4, 6 and p_{sd} for n = 3, 5, 7), then we can express the cost of initial and terminal stored energy f_s from (3.9) as

$$
\begin{aligned}
f_{\mathrm{s}}(s_0, p_{\mathrm{sc}}, p_{\mathrm{sd}}) &= C_{\mathrm{s}0}^{\mathsf{T}} s_0 - v_S(x) \\
&= C_{\mathrm{s}0}^{\mathsf{T}} s_0 - (C_{\mathrm{ts}0}^{\mathsf{T}} s_0 + C_{\mathrm{tsc}}^{\mathsf{T}} p_{\mathrm{sc}} + C_{\mathrm{tsd}}^{\mathsf{T}} p_{\mathrm{sd}})
\end{aligned} \tag{3.91}
$$

where

$$C_{\mathrm{ts}0} = A_1^{\mathsf{T}}[\eta_{\mathrm{out}}] C_{\mathrm{s}} \tag{3.92}$$

$$C_{\mathrm{tsc}} = \bar{A}_2^{\mathsf{T}}[\eta_{\mathrm{out}}] C_{\mathrm{s}} + \bar{A}_4^{\mathsf{T}}[\eta_{\mathrm{out}}] C_{\mathrm{sc}0} + \bar{A}_6^{\mathsf{T}}[\eta_{\mathrm{out}}] C_{\mathrm{sc}k} \tag{3.93}$$

$$C_{\mathrm{tsd}} = \bar{A}_3^{\mathsf{T}}[\eta_{\mathrm{out}}] C_{\mathrm{s}} + \bar{A}_5^{\mathsf{T}}[\eta_{\mathrm{out}}] C_{\mathrm{sd}0} + \bar{A}_7^{\mathsf{T}}[\eta_{\mathrm{out}}] C_{\mathrm{sd}k}. \tag{3.94}$$

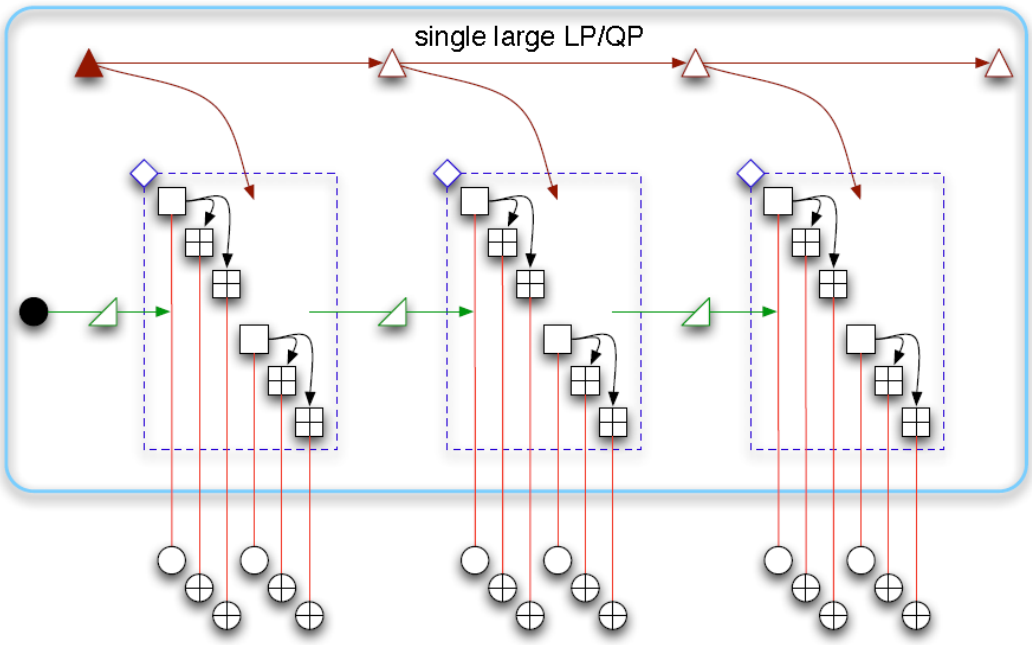

Figure 3-2: Problem Decomposition

3.6 Problem Decomposition

Such a formidable problem is hard to solve for realistic system sizes using an island representation, as has been done in our earlier work. For example, the IEEE 30 bus system with a 24-hour horizon, seven scenarios per time period and 10 contingencies, results in 1,848 coupled power flows, and an island representation would involve a 55,440 bus system with 1,848 islands and many unusual constraints and additional variables. Although improvements in the solvers employed by MATPOWER allow it

to solve problems of this size, larger systems with more contingencies and efficiency considerations suggest that the problem should be decomposed.

In the current design, the decomposition is done by duplicating the variables representing all of the active power injections. One set is used in individual AC OPF problems, each representing a specific scenario or contingency in a specific period. The other set is used in a central coordination quadratic program containing all of the intertemporal and inter-flow constraints and their corresponding variables and costs. The overall structure is illustrated in Figure 3-2. With this decomposition scheme, the granularity on the level of a single OPF allows for massive parallelization and the central quadratic program, although large, can be solved up to realistic-sized problems with the current generation of QP and LP solvers. Coordination occurs only at the level of the two copies of the set of all active injections.

Essentially, all traditional OPF constraints (3.11) - (3.12) are imposed on the sets of variables (θ^{tijk}, V^{tijk}, π^{tijk}, ρ^{tijk}), where π^{tijk} and ρ^{tijk} are the active and reactive injections, whereas constraints (3.13) - (3.30), together with network-like proxy constraints to limit the search space on p^{tijk}, and the original cost are imposed on variables (p, q, p_c, p_+, p_-, r_+, r_-, s_+, s_-, δ_+, δ_-). Then, quadratic coordination costs arising from an augmented Lagrangian coordination scheme are imposed on the active injections to force equality of p^{tijk} and π^{tijk}. Thus, the costs for each of the OPFs is purely made from the coordination costs

$$\sum_i \{\frac{b}{2}(\pi^{tijk})^2 + [\lambda^{tijk} - b\pi^{tijk}_{\text{old}} + c(\pi^{tijk}_{\text{old}} - p^{tijk}_{\text{old}})]\pi^{tijk}\} \qquad (3.95)$$

Where λ^{tijk} are the coordination multipliers, c is the quadratic augmentation term coefficient, so $c(\pi^{tijk}_{old} - p^{tijk}_{old})\,\pi^{tijk}$ is the linearization of this term about the previous iteration's values of (π^{tijk}, p^{tijk}), b is the coefficient of the quadratic regularization term $\frac{b}{2}(\pi^{tijk} - \pi^{tijk}_{old})^2$; it has a damping effect in the trajectory of the coordination multipliers, a useful feature if problem costs are rather flat. Similarly for the QP, the cost (3.4) is modified to include the terms

$$\sum_t \sum_j \sum_k \sum_i \{\frac{b}{2}(p^{tijk})^2 + [-\lambda^{tijk} - bp_{\text{old}}^{tijk} + c(\pi_{\text{old}}^{tijk} - p_{\text{old}}^{tijk})]p^{tijk}\} \qquad (3.96)$$

An algorithm for solving the problem with this decomposition is as follows:

1. Initialize (λ^{tijk}), perhaps by solving the large QP without the coordination costs and with linearized network constraints; the (λ^{tijk}) take the values of the nodal prices at the active injection buses. This also assigns initial values to (p^{tijk}). Similarly, obtain initial values for (π^{tijk}), perhaps by solving each individual OPF with just the original fuel cost.

2. Compute the mismatches π^{tijk} - p^{tijk}.

3. Update the coordination multipliers according to the mismatches, perhaps by

$$\lambda^{tijk} \leftarrow \lambda^{tijk} + \beta(\pi^{tijk} - p^{tijk}) \qquad (3.97)$$

   where β is a step-control parameter.

4. $\pi_{old}^{tijk} \leftarrow \pi^{tijk}$

   $p_{old}^{tijk} \leftarrow p^{tijk}$.

5. Solve one OPF for each of the flows considered in the problem, with cost (3.95) and restrictions (3.11) - (3.12); obtain new (π^{tijk}).

6. Solve one large QP with cost (3.4) ammended with addition (3.96), constraints (3.13){(3.30), and proxy network constraints such as

$$-0.1P_D^{tijk} \leq P_D^{tijk} - \sum_i p^{tijk} \leq 0.1P_D^{tijk} \qquad (3.98)$$

   where P_D^{tijk} is the system demand in flow (*tijk*) . From this, obtain new (p^{tijk}).

7. Compute mismatches π^{tijk} - p^{tijk}; if any are larger in magnitude than some tolerance, go to step 3 and repeat.

8. From solution, compute all quantities not expressly obtained, such as expected dispatches and expected storage values.

Chapter 4: Evaluation Study of the Incorporation of Transient Stability Constraints into Optimal Power Flow

4.1 Introduction

In this chapter, we provide a detailed investigation of the widely used fixed-threshold proxi on its performance in enforcing transient stability constraints in TSCOPF. The question of accuracy and reliability from using this fixed-threshold proxi will be addressed through extensive time-domain simulation studies. The computations and analysis of the exact threshold values under different test systems, loading conditions, network topology and contingencies is conducted. To obtain the exact threshold values, this chapter presents an exact method using the framework of stability region. A stability-region framework for TSCOPF is also established to provide a more accurate expression of transient stability constraints in the TSCOPF formulation.

Our evaluation study shows that the exact threshold value is not a constant, as assumed in the literature, and can vary from 80 to 190 degrees. This leads to the following issues related to the current fixed-threshold proxi: (i) the current common threshold values of 100º-120º can be very conservative as the correct value can be as large as 190º, (ii) the common threshold values can also be very optimistic as the correct value can be as small as 80º in some systems, (iii) the exact threshold value is not a constant and depends on contingencies, loading conditions and network topology, and (iv) the integration time of 2 to 5 seconds can be problematic for the cases with multi-swing instability. It is numerically shown that using the same fixed threshold value can lead to both severe underestimate and overestimate transient stability assessments. Instead of using the same predetermined and fixed thresholds in the inequalities of every system and contingency, we suggest using adaptive limits that depend on the overall system dynamics.

4.2 TSOPF Problem Formulations

The TSCOPF problem can be formulated by incorporating a set of transient stability constraints into the conventional OPF formulation, which can be described as follows:

4.2.1 Conventional OPF Formulation

$$\text{Min} \quad f(P_g) \tag{4.1}$$

$$\text{S.T.} \quad P_g - P_L - P(V,\theta) = 0 \tag{4.2}$$

$$Q_g - Q_L - Q(V,\theta) = 0 \tag{4.3}$$

$$|S(V,\theta)| - S^{\max} \le 0 \tag{4.4}$$

$$V^{\min} \le V \le V^{\max} \tag{4.5}$$

$$P_g^{\min} \le P_g \le P_g^{\max} \tag{4.6}$$

$$Q_g^{\min} \le Q_g \le Q_g^{\max} \tag{4.7}$$

Where $f(\cdot)$ is an objective function; P_g and Q_g are the vectors of generator active and reactive power output, respectively; $P_g^{\max}$ and $P_g^{\min}$ are the upper and lower bounds of real power output while $Q_g^{\max}$ and $Q_g^{\min}$ are the bounds for reactive power output; P_L and Q_L are real and reactive power loads; $P(V,\theta)$ and $Q(V,\theta)$ are the real and reactive network injections; $S(V,\theta)$ is a vector of apparent power across the transmission lines whose thermal limits are restricted by $S^{\max}$; V and θ are the vectors of bus voltage magnitudes and angles with associated lower and upper limits of $V^{\min}$ and $V^{\max}$, respectively. P_g, Q_g, V and θ are the free variables in the problem.

4.2.2 Transient Stability Constraints

The constraints associated with transient stability consist of swing equations (a set of DAEs) that describe the generator rotor angle deviation after a disturbance and stability limit criteria to determine whether the system is stable.

Swing equations

The classical model of a synchronous generator is adopted, and loads are modeled as constant impedances. The rotor angle deviation of the *i*-th synchronous generator can be expressed by differential equations as follows [15]:

$$\begin{aligned} \dot{\delta}_i &= \omega_i \\ M_i\dot{\omega}_i &= P_{mi} - P_{ei}(\delta) - D_i\omega_i, \quad i = 1,...,n \end{aligned} \tag{4.8}$$

where, $P_{ei}(\delta) = E_i \sum_{k=1}^{n} E_k (G_{ik}\cos\delta_{ik} + B_{ik}\sin\delta_{ik})$ is the electrical power at machine i, E_i is the constant voltage behind direct axis transient reactance. D_i and M_i are the damping ratio and inertia constant of machine i .and P_{mi} is the mechanical power. $Y = (Y_{ij})_{n\times n} = (G_{ij} + jB_{ij})_{n\times n}$ is the reduced admittance matrix.

Stability Region

A stability-region framework is proposed to provide a more accurate expression of transient stability constraints in the TSCOPF formulation.

Let us consider a general nonlinear dynamical system described by:

$$\dot{x} = f(x) \tag{4.9}$$

An *equilibrium point* is a solution to the equation $0 = f(x)$. An *assymptotically stable equilibrium* point x_s of (4.9) is the point where all the eigenvalues of the Jacobian matrix have negative real parts. The flow or trajectory of the system (4.9) is the solution to (4.9) at time t starting at x, and it is denoted by $\phi(t, x)$. The stability region of an asymptotically stable equilibrium point (SEP) x_s can be expressed as:

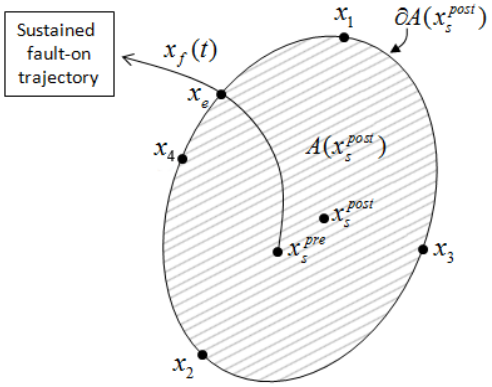

Fig. 4-1: The sustained fault-on trajectory $x_f(t)$, starting from the pre-fault SEP x_s^{pre}, moves toward the stability boundary $\partial A(x_s^{post})$ and intersects it at the exit point, x_e. x_s^{pre} is assumed to lie inside the stability region of post-fault SEP $A(x_s^{post})$.

$$A(x_s) = \{x : \phi(t, x) \to x_s, \quad \text{as } t \to +\infty\} \tag{4.10}$$

To analyze transient stability due to a fault, the system is considered to go through three stages: pre-fault stage, fault-on stage and post-fault stage. The fundamental issue of transient stability analysis is whether the system trajectory, starting at the post-fault initial state $x(t_{cl})$, will settle down to x_s^{post}. Transient stability analysis is to determine whether the initial point of the post-fault trajectory is located inside the stability region of the equilibrium point x_s^{post}. It can be mathematically expressed by checking the following condition:

$$x(t_{cl}) \in A(x_s^{post}) \tag{4.11}$$

To be practical we let N be the set of the contingencies being considered in a TSCOPF problem, and $A(x_{si}^{post})$ $i \in N$ denotes the stability region of x_{si}^{post} associated with the contingency i. Then the mathematical expression of the transient stability constraints in TSCOPF based on the stability-region framework can be described as follows.

$$x_i(t_{cl}) \in A(x_{si}^{post}) \quad \forall i \in N \tag{4.12}$$

In summary, the TSCOPF problem can be formulated as follows:

Minimize	(4.1)	
Subject to	(4.2)-(4.7)	
	(4.8) and (4.12)	(4.13)

4.3 Proxi for Transient Stability Constraints and Numerical Issues

Solving a TSCOPF problem as formulated in (4.13) can be very challenging because (i) there are infinite-dimensional variables, equalities and inequalities associated with the swing curves (4.8), and (ii) the expression in (4.12) does not have a closed-form analytical expression. To avoid these two numerical difficulties, many researchers consider the transient stability constraints in TSCOPF through discretized swing curves [6], [8]-[15] and constrain the relative rotor angle within a predefined limit [6]-[16]. By using the implicit trapezoidal rule [6] or Taylor series expansion, differential equations can be discretized and converted into numerically equivalent algebraic equations, which can be easily included in the OPF formulation. The following criterion is widely used in TSCOPF research as a proxi for ensuring system transient stability.

$$\begin{aligned} &\left|\delta_i(t)-\delta_{COI}(t)\right|_{\max} \le \delta_{\max} \\ &0 \le t \le t_{\max} \end{aligned} \tag{4.14}$$

where $\delta_i(t)$ is the rotor angle of machine *i* at time *t*. $\delta_{COI}(t)$ is the center of inertia (COI) reference angle. $\delta_{\max}$ is a fixed angle threshold, normally set between 100° - 120°. $t_{\max}$ is the total integration time. In TSCOPF, $t_{\max}$ is typically set to 2-5 seconds. This constraint requires the rotor angle deviation of all machines, with respect to the center of inertia, to be no greater than $\delta_{\max}$ at all time. If the condition is satisfied, the operating point is considered transiently stable.

Although the proxi (4.14) has been commonly used in the TSCOPF formulation, there are several technical and numerical issues that must be addressed:

1. Accuracy and validity of the criterion – The inequality criterion in (4.14) is merely an approximated and simplified form of the real expression of transient stability in (4.12). Moreover, the predefined thresholds, or $\delta_{\max}$ in (4.14), are heuristically chosen and vary considerably from 90° to 140° in the literature [6]-[16].

2. Computational burden – The discretization of the differential equations introduces a large number of new equations and variables for each time step. The number multiplies when multiple contingencies or a longer integration duration is being considered.

3. Convergence – A large number of constraints and variables may cause a TSCOPF program to diverge.

4. Scalability – Although in theory this guideline can be extended to consider multiple contingencies or detailed generator models, it is computational impractical due to the extra computational burden.

In this chapter, we will address the issue of accuracy and, to a certain extent, address the issue of computational burden.

4.4 Method for Computing Exact Threshold

An exact method is proposed to compute the exact thresholds using the framework of stability region. The exact threshold represents the highest value of rotor angle deviation, with reference to the center of inertia (COI), such that the post-fault trajectory remains in the stability region of the post-fault system and converges to the post-fault stable equilibrium point. The method for computing the exact threshold values is presented below.

Given: A contingency with a specified fault-on trajectory and a specified post-fault SEP.

Method: Computing exact threshold values for angle inequalities

Step 1: Compute the exact critical clearing time (CCT) in the direction of fault-on trajectory by using a time-domain method.

Step 2: Perform a time-domain numerical integration starting from an initial point with fault clearing time slightly less than the critical clearing time. This step produces a critically stable post-fault trajectory.

Step 3: Identify the maximum angle deviation $\delta_{\max}^{exact}$ along the critically stable post-fault trajectory, which can be found at the highest or lowest peak of the trajectories.

Output: The exact threshold value of the contingency in the context of angle inequality (4.14) is $\delta_{\max}^{exact}$.

Table 4-1: Clearing Times And The Peaks Of Post-Fault Trajectories
Wscc9, Fault-Bus: 9, Tripped-Line: 9-6

Clearing times	Peak* (degree)
0.2429 = CCT	166.16
0.202	100.00
0.20	98.27
0.15	66.58
0.10	45.95
0.07	37.15

* A peak value represents the maximum amplitude of post-fault trajectories

One distinguished feature of the proposed method is that it reflects the network topology, loading conditions, etc. and is based on the exact relevant stability boundary of the transient stability models [23]. It has been observed from our numerical results that the peak value of the angle deviations of post-fault trajectories strictly increases as the fault clearing time increases. The simulation results summarized in Table 4-1 and Figure 4-2 confirm this observation. This observation shows that the highest rotor angle deviation, or the exact threshold, can be obtained from a critically stable post-fault trajectory whose initial point lies just inside the stability boundary of the post-fault system.

4.5 Proxi from Stability Region Viewpoint

To address the accuracy issue of using (4.14) in place of (4.12), we present a numerical result showing the performance of the fixed-threshold proxi in estimating CCTs. The WSCC9 [22] with constant impedance loads and a uniform damping of 0.1 is considered.

Bus 9 is shorted during the fault-on period and line 9-6 is tripped by the protection system. The actual CCT of this system and contingency is 0.2429 second. Figure 4-3 and 4-4 show the same set of post-fault trajectories in different spaces and representations. Figure 4-3 displays post-fault stable and unstable trajectories in the state space, along with the exact stability region of the post-fault SEP. The stable trajectory moves inside the stability region and eventually converges to the post-fault SEP. On the other hand, the unstable trajectory, starting from the outside the stability region, directly diverges to infinity. Figure 4-4 contains the same stable and unstable trajectories as shown in Figure 4-3; however they are represented as swing curves versus time.

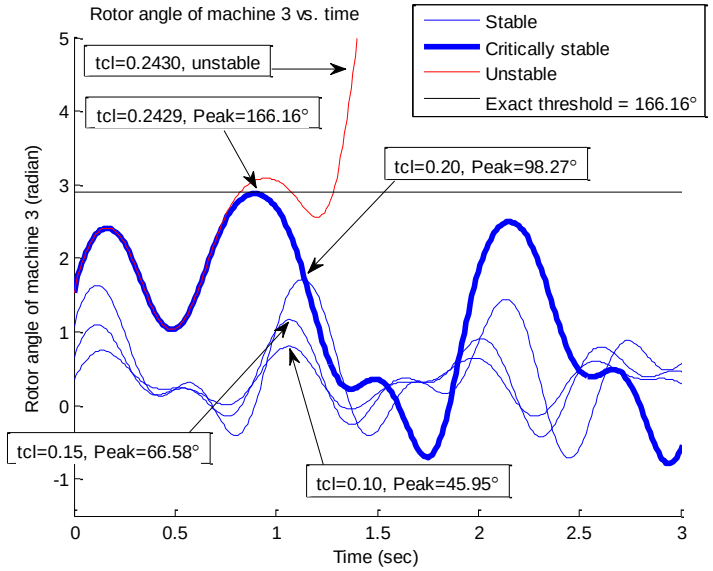

Figure 4-2: The exact threshold value can be obtained at the highest peak of the critically stable post-fault trajectory. The fault-on trajectory crosses the stability boundary at the critical clearing time of 0.2429 second

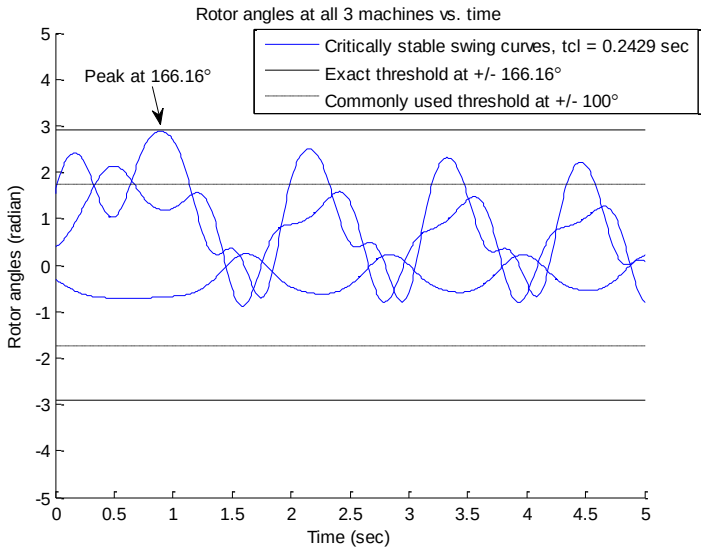

Figure 4-3: Critically stable swing curves when clearing time is 0.2429 second, slightly less than the CCT. The peak of the rotor angles is observed at 2.9 radian or 166.16°.

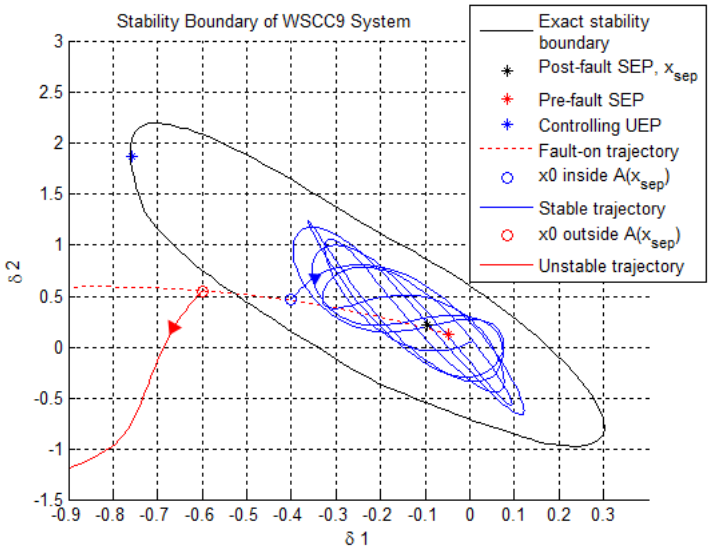

Figure 4-4: A stable trajectory travelling inside the stability region in the state space, while an unstable trajectory lying outside the stability region moves away from it.

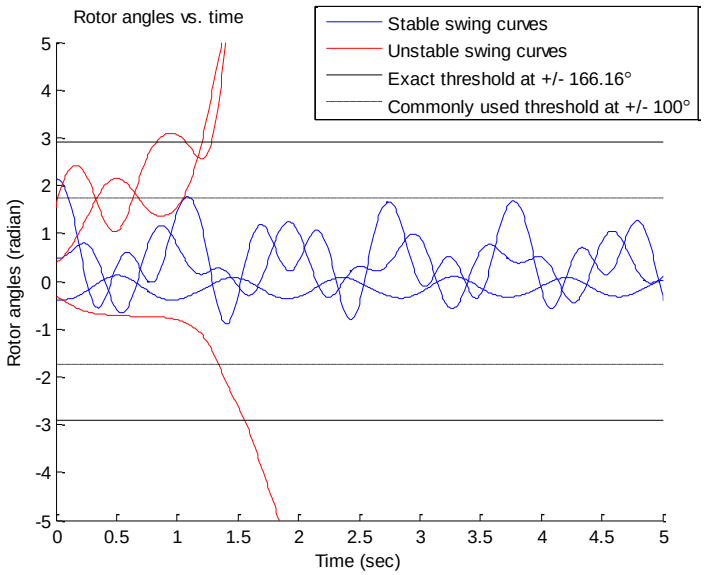

Figure 4-5: The stable swing curves and unstable stable swing curves in Figure 4-2 as a function of time. The exact threshold value of 2.9 radians of 166.16 degrees was found at CCT = 0.2429 second by an exact method, and compared to the commonly used threshold of 100°.

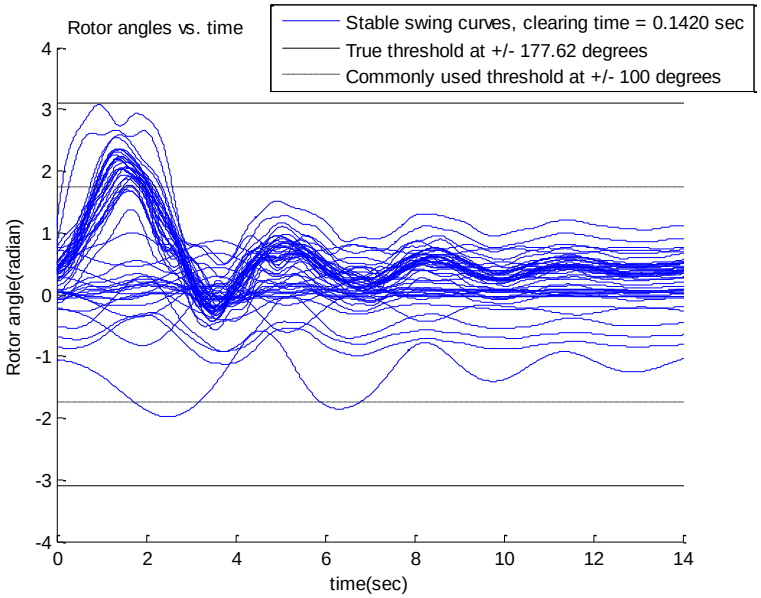

Figure 4-6: At fault clearing time = 0.1420 second, a stable post-fault trajectory is confined in the correct limits of +/- 177.62°.

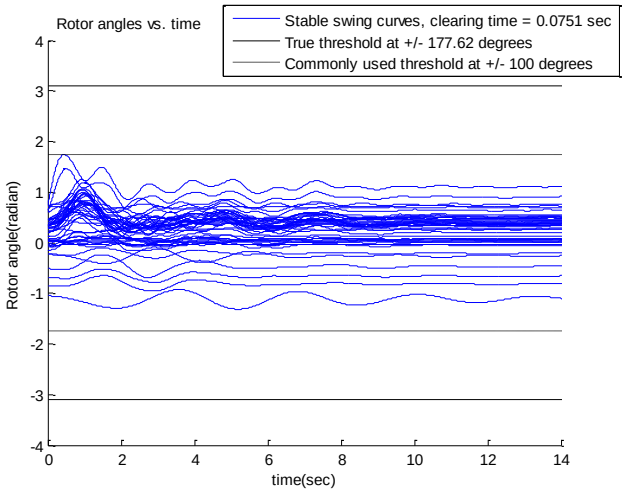

Figure 4-7 At fault clearing time = 0.110 sec, a stable post-fault trajectory is confined in the commonly used limits of +/- 100°.

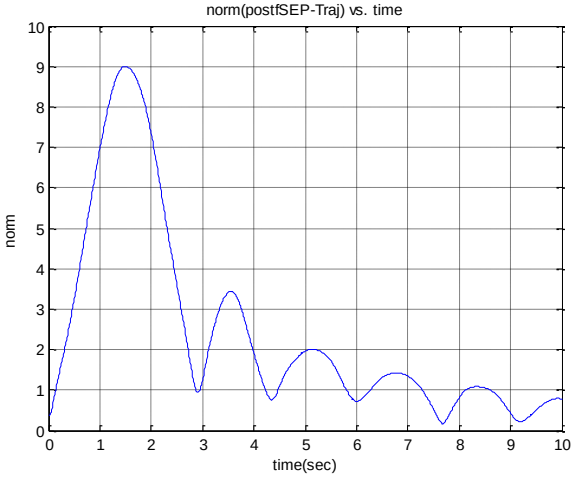

Figure 4-8: Fault clearing time = 0.1420 sec, the post-fault trajectory converges to a post-fault SEP

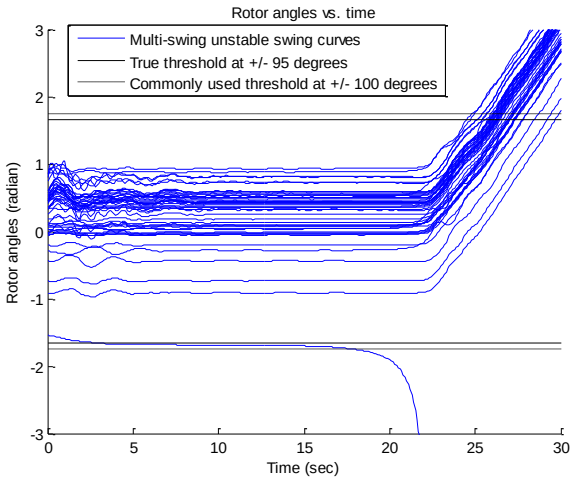

Figure 4-9: A multi-swing unstable post-fault trajectory can take more than 15 seconds before encountering an angle separation.

Using the proposed exact method, we can obtain a critically stable post-fault trajectory when the fault clearing time is 0.2429 second, and the exact threshold value of 166.16°, see Figure 4-2 or 4-5. When compared to the exact value, the common fixed-threshold of 100° is very conservative with a relative threshold error of 39.82%. The estimated CCT associated with the 100° threshold is equal to the highest fault-clearing time such that the post-fault trajectories lie entirely in the +/- 100° range. In this contingency, the estimated CCT associated with the 100° threshold is 0.202 second, see Table 4-1. This translates to a 13.54% relative error of estimated CCT by the 100° fixed threshold proxi.

4.6 Numerical Study on Threshold Values

A time-domain study on the IEEE145 test system [21] was conducted to address the following issues associated with the commonly used fixed-threshold proxi for transient stability constraints in TSCOPF.

1. The predefined threshold value is heuristically selected in the range of 100°-120°, through generalized estimations of swing curves. It will be shown that the exact threshold value of a system can vary from 80° to 190°, depending on several factors such as types of contingency, loading conditions, and network topology. The question is, if the same threshold value is used for every system and contingency, as suggested

in the literature, will it affect the accuracy of the proxi in enforcing transient stability in TSCOPF? If it does, how large the errors can be expected?

2. Due to the highly-computational nature of this solution method, longer integration times are undesirable. As can be seen in [6, 10, 11, 12], only 2-5 seconds of integration time is performed to solve TSCOPF problems. This practice may become problematic in the case of multi-swing instability, where the rotor angle separations usually take longer to occur. We will address this issue and find out the outcome of using a short integration time along with a fixed-threshold proxi to solve TSCOPF in this situation.

We next show the numerical results on the IEEE145 test system. Loads are modeled as constant impedances and the uniform damping of 0.1 is considered. Bus 7 is shorted during the fault-on period and line 7-6 is tripped to clear the fault. The actual critical clearing time is 0.1424 second.

Table 4-2: Relative Error Percentage of Estimated CCT's

	$\delta_{max} = 100°$	$\delta_{max} = 120°$
Fixed threshold	100°	120
Exact threshold	177.62°	177.62°
Threshold relative error %	43.70	32.44
Estimated CCT	0.0751	0.1100
Actual CCT	0.1424	0.1424
CCT relative error %	47.26	22.75

4.6.1 Underestimate of Threshold and CCT

Figure 4-6 shows a critically stable post-fault trajectory when the fault clearing time is 0.1420 second, slightly lower than the CCT. All 50 machine rotor angles are presented in Figure 4-6. Figure 4-7 displays the displacement from the post-fault SEP to the trajectory. It confirms that this trajectory is stable and asymptotically converges to the post-fault SEP. Figure 4-6 presents an example of a stable trajectory which the TSCOPF criterion in (4.14) with 100° fixed threshold considers unstable. The rotor angles at the following buses are all larger than 100° or 1.7453 radian at some points along the curves: 2, 3, 4, 6,

7, 8, 9, 12, 13, 14, 15, 16, 17, 19, 20, 21, 22, 25, and 26. To confine the whole swing curves in the +/- 100° limits, the fault clearing time has to be significantly reduced to 0.0751 second, see Figure 4-7. We show in Table 4-1 that the peak value of swing curves strictly increases as the fault clearing time increases. This means that, for this system and contingency, using a 100° threshold is equivalent to restricting the fault clearing time to be equal or less than 0.0751 second. In other words, it is equivalent to having an estimated CCT of 0.0751 second. Table 4-2 contains the relative errors of CCTs and threshold values when fixed thresholds of 100° or 120° are used in the TSCOPF proxi. This numerical result shows that using a fixed-threshold proxi (i.e. 100°) in TSCOPF can lead to a severe underestimate of the exact threshold and CCT. The relative error for threshold value in this case can be as high as 43.70 %. In the context of optimization problems, this means that a large number of feasible solutions, those that are transiently stable, may be considered unstable and disregarded due to the predetermined threshold value being too small and conservative.

4.6.2 Overestimate of Threshold and CCT

The test system is IEEE145 with constant impedance loads and a uniform damping of 0.1. Bus 8 is shorted during the fault-on period and line 8-7 is tripped to clear the fault. A high loading condition is considered in this case. The actual CCT is 0.071 second. Using the proposed exact method, we found the exact threshold value of 95°. Figure 4-9 shows a multi-swing unstable swing curve when the fault clearing time is 0.072 second, slightly larger than the actual CCT. It can be observed that the separation of the rotor angles does not occur until after 15 second in the post-fault stage. If the common 100° threshold is considered in (4.21), the violation of the inequality will occur at 17.35 second. This becomes a problem because, as described in section III, the post-fault integration time is normally limited to 2-5 seconds. This means no violation will occur within this period and the angle separation at 17.35 second will not be detected. Using the correct threshold value of 95° will however result in a correct detection at 2.46 second, see Figure 4-9. This is an example where using a fixed-threshold proxi (i.e. 100°) can lead to an overestimate of CCT, and a false assessment. In the context of optimization problems, this means that some infeasible solutions, those that cause transient instability, may be considered feasible when solving for an optimal solution.

In summary, we present the numerical results to show that if the threshold value in (4.14) is predetermined and fixed for every case and contingency, it may lead to both severe underestimate and overestimate assessments in TSCOPF. It is also shown that using the exact threshold values in, which can be found by the proposed exact method, can eliminate these shortcomings.

4.7 Accurate Thresholds under Different Conditions

It has been shown that the correct threshold value in (4.14) can be different for each system and contingency, and that using a fixed threshold, as suggested in the literature, can lead to an inaccurate proxi for transient stability constraints in TSCOPF. We next examine the exact threshold values under the following different conditions: (i) types of contingencies, (ii) loading conditions, and (iii) severe contingencies. The numerical study on the IEEE145 shows that the exact threshold values vary significantly from 80°-190° under different system conditions. This emphasizes the importance in adjusting $\delta_{\max}$ of (14) in accordance to the system's dynamics and contingencies.

4.7.1 Type of Contingencies

Table 4-3: Exact Threshold Values in Different Types of Contingencies

Contingencies	CCT(sec)	Threshold (degree)
Secure	CCT > 0.2	
59: 59-72	0.2415	174.24
116:115-116	0.2866	192.63
1: 1-2	0.4067	176.47
8: 7-8	1.0596	165.81
11: 9-11	2.4959	172.69
Average threshold = 176.24 degree		
Critical	0.1 < CCT < 0.2	
6: 7-6	0.1671	190.11
7:7-6	0.1424	182.66
104: 7-104	0.1681	195.03
98: 58-98	0.1208	144.10
89: 59-89	0.1402	155.10
Average threshold = 170.52 degree		
Insecure	CCT < 0.1	
17: 17-22	0.0835	139.74
33: 33-34	0.0676	115.22
99: 36-99	0.0419	110.70
2: 2-113	0.0693	113.45
Average threshold = 119.78 degree		

Table 4-3 shows the correct threshold values when different types of contingencies are considered. Since the protection system is normally activated within 5-8 cycles, or 0.0833-0.1333 second after a disturbance, any case with a CCT lower than 0.1 second will be considered insecure. If the CCT lies between 0.1 and 0.2, it will be considered critical. When the CCT is greater than 0.2, that contingency is considered secure. We can see that the threshold values are smallest in the insecure group with the average value of 119.78°, followed by 170.52° of the critical group. The secure group has the highest average value of 176.24°. It can be observed that as the CCT decreases, the threshold tends to decrease in general.

This numerical result shows that true threshold value for each contingency is different and it is related to the value of the critical clearing time. It can be observed that the exact threshold value decreases as CCT decreases.

4.7.2 Loading Conditions

The effect of loading conditions on the threshold value is studied and presented in Table 4-4. Three contingencies (one from each contingency group) are considered in this study. It can be observed from the results that as loads increase, both CCTs and threshold values strictly decrease. The results are uniform among all three types of contingencies. Note that the insecure contingency contains less data than the other two due to the lowest load margin. The result illustrates how the loading condition has a direct impact on the exact threshold value of each contingency. As loads increase, the exact threshold value also decreases.

Table 4-4: Exact Values of Thresholds in Different Loading Conditions

Loading	CCT(sec)	Threshold (degree)
Secure Contingency: 8:7-8		
Original	1.0596	165.81
+5%	0.7708	164.55
+10%	0.5433	154.13
+15%	0.3686	127.83
+19%	0.166	107.49
+19.5%	0.075	104.11
+20%	0	-
Critical Contingency: 7:7-6		
Original	0.1424	182.66
+5%	0.1167	171.03
+10%	0.0837	145.36
+14%	0.0311	126.28
+15%	0	-
Insecure Contingency: 17:17-22		
Original	0.0835	139.74
+5%	0.0431	119.63
+6%	0.0221	97.92
+7%	0	-

Table 4-5: Exact Values of Thresholds in Severe Contingencies

Contingency	CCT(sec)	Threshold (degree)
Line out: 17-22		
59: 59-72	0.0209	90.46
115: 115-116	0.0198	89.76
1: 1-2	0.0212	92.48
6: 7-6	0.0164	83.23
98: 58-98	0.0173	85.49
89: 59-89	0.0103	79.41
104: 7-104	0.0115	81.69

4.7.3 Severe Contingencies

Table 4-5 presents the threshold values of some severe contingencies of IEEE145. Line 17-22 is permanently taken out when the test for other contingencies is run. It can be observed that the exact threshold values of all the cases are below 100°. If the criterion (4.14) is used with a fixed $\delta_{\max} = 100°$, and if the multi-swing instability is taken into consideration, these insecure contingencies may be considered secure by the proxi. To avoid this type of false assessment in TSCOPF, either the integration time must be extended well beyond 5 seconds, or an exact threshold value must be used.

4.8 TSCOPF using Different Threshold Values

Through a numerical study on several single-contingency TSCOPF problems, we demonstrate that the TSCOPF solution can be significantly different when different values of threshold in (4.14) are considered. The test system is WSCC9 with a uniform damping of 0.05. The system cost function can be found in [24]. The results show that the objective function values at optimal power flow solutions vary considerably under different fixed threshold values. Figure 4-10 displays the single-contingency TSCOPF solutions associated with three different values of fixed threshold. It can be observed that the objection function can be improved by adjusting the fixed-threshold value in (4.14). The costs are highest when the threshold value is 100°, and gradually decrease as the threshold value is raised. The objective function values appear be the lowest or the best when the threshold value is relaxed to 160°, the highest of the three values we tested. Regarding the system transient stability, the stability requirement is satisfied in all threshold values and contingencies as we can see that the CCTs are all greater than the required 0.20 second. The CCTs however appear to be on the conservative side in all cases, with 100° threshold being the most conservative.

This result shows that if the threshold value in (4.14) is chosen without the actual knowledge of system dynamics, it may cause unnecessary conservativeness and degradation of the optimal solution. This demonstrates the importance of adjusting the threshold values in accordance to the dynamics of studied systems. By properly reflecting

accurate threshold values, the TSCOPF solutions can be improved without losing system transient stability.

4.9 Conclusion

This chapter provides a critical evaluation of the fixed-threshold proxi for transient stability constraints in TSCOPF. An exact method to determine exact threshold values is developed based on the stability region framework. The proposed method has been applied to derive exact threshold values of power system under different test systems, loading conditions, network topology and contingencies. Our evaluation study shows that the exact threshold values are not constant, as assumed in the literature, and can vary from 80 to 190 degrees depending on several factors such as types of contingency, loading conditions, and network topology. By using the commonly used fixed-threshold proxi (i.e. 100° or 120°) to express transient stability in TSCOPF, it can lead to severe underestimate assessments as well as overestimate assessments. We also demonstrate that if the threshold value in the proxi is chosen without the actual knowledge of system dynamics, it may lead to unnecessary conservativeness of transient stability and degradations of the optimal solutions.

We emphasize that the current fixed-threshold proxi used in the TSCOPF literature is merely a simplified form of the real expression of transient stability in power systems. Therefore, it may be subject to errors and incorrect assessments. To achieve accurate results in TSCOPF, it is critical that the threshold value is adjusted based on the system dynamics and its loading conditions, and this adjustment should be based on the knowledge of stability regions. The proposed method can meet this requirement.

Chapter 5 A Novel BCU-Based OPF Method for Large-Scale Power Systems with Transient Stability Constraints

5.1 Introduction

This chapter proposes a novel BCU-based TSCOPF method that overcomes these issues through the combination of a fast screening algorithm by BCU method [46] and a BCU-based computation of accurate system-dependent threshold values.

The BCU method is incorporated into the proposed method to reduce the computational burden by eliminating irrelevant contingencies. It screens out the majority of secure contingencies and prevents the TSCOPF formulation from considering unnecessary contingencies. A BCU-based scheme is proposed to provide an efficient way to compute system threshold values. Although a scheme for computing exact threshold values has been proposed in [40], it is based on a time-domain approach which is computationally expensive and impractical for large-scale power systems. To overcome this limitation, a BCU-based scheme is proposed for fast computation of system threshold values. The scheme is tested on several case studies and shown to yield fairly accurate and conservative estimations of the exact threshold values. The CPU time required by the proposed BCU-based scheme is remarkably reduced when compared with the time-domain-based method.

The unique features of the proposed BCU-based TSCOPF method are as follows:

(uf1) it enables the TSCOPF to solve practical power systems with a large contingency list,

(uf2) it provides accurate threshold values which improves the accuracy of transient stability constraints and quality of the TSCOPF solution,

(uf3) it can lead to better optimal solutions (in the context of objective function values)

(uf4) it can be applied to any discretization- based TSCOPF methods.

The numerical results show significant improvement in both computational capability and solution quality in all case studies. These promising results show that the proposed BCU-based method is suitable for solving the solution of large-scale TSCOPF problems with large contingency lisst.

5.2 TSCOPF Problem Formulations

The TSCOPF problem can be formulated as a large-scale nonlinear programming problem associated with DAE constraints [27].

$$\begin{aligned} \min_{\mathbf{x},\mathbf{z}} \quad & f(\mathbf{x},\mathbf{z}) \\ s.t. \quad & \mathbf{H}_0(\mathbf{x},\dot{\mathbf{x}},\mathbf{z}) = 0 \\ & \mathbf{G}_0(\mathbf{x},\dot{\mathbf{x}},\mathbf{z}) \le 0 \end{aligned} \tag{5.1}$$

where vector **x** are state variables such as voltage magnitudes and angles, while **z** are the control variables such as power outputs, transformer tap ratios, phase shifter positions, etc.

5.2.1 Objective function

The objective functions in TSCOPF are generally the same as those in conventional OPF. In this chapter, minimization of generation cost functions is considered.

$$f(x) = \sum_{i=1}^{ng} \left(a_i P_{gi}^2 + b_i P_{gi} + c_i \right) \tag{5.2}$$

5.2.2 Conventional OPF equality and inequality constraints

1) Power flow equations:

$$\begin{aligned} \mathbf{P_g} - \mathbf{P}_l - P(\mathbf{V},\boldsymbol{\theta}) = 0 \\ \mathbf{Q_g} - \mathbf{Q}_l - Q(\mathbf{V},\boldsymbol{\theta}) = 0 \end{aligned} \tag{5.3}$$

where $\mathbf{P_g}$ and $\mathbf{Q_g}$ are the vectors of generator active and reactive power outputs, while $\mathbf{P}_l$ and $\mathbf{Q}_l$ are real and reactive power loads. $\mathbf{V},\boldsymbol{\theta}$ are the vectors of bus voltage magnitudes and angles.

2) Static security constraints:

$$\begin{aligned}
&\mathbf{P_g}^{\min} \le \mathbf{P_g} \le \mathbf{P_g}^{\max} \\
&\mathbf{Q_g}^{\min} \le \mathbf{Q_g} \le \mathbf{Q_g}^{\max} \\
&\mathbf{V}^{\min} \le \mathbf{V} \le \mathbf{V}^{\max} \\
&\left|\mathbf{S}(\mathbf{V},\boldsymbol{\theta})\right| - \mathbf{S}^{\max} \le 0
\end{aligned} \tag{5.4}$$

5.2.3 Transient Stability Constraints

The rotor angle deviation of the *i*-th synchronous generator can be expressed by differential equations as follows [48]:

$$\begin{aligned}
&\dot{\delta}_i = \omega_i \\
&M_i\dot{\omega}_i = P_{mi} - P_{ei}(\delta) - D_i\omega_i, \quad i = 1,...,ng
\end{aligned} \tag{5.5}$$

where, $P_{ei}(\delta) = E_i \sum_{k=1}^{ng} E_k (G_{ik}\cos\delta_{ik} + B_{ik}\sin\delta_{ik})$ is the electrical power at machine i, E_i is the constant voltage behind direct axis transient reactance. D_i and M_i are the damping ratio and inertia constant of machine i. and P_{mi} is the mechanical power. $Y = (Y_{ij})_{n\times n} = (G_{ij} + jB_{ij})_{n\times n}$ is the admittance matrix.

Let us consider a general nonlinear dynamical system described by:

$$\dot{x} = f(x) \tag{5.6}$$

An *equilibrium point* is a trivial solution of (5.6). An *assymptotically stable equilibrium* point x_s of (5.6) is the point at which all the eigenvalues of the corresponding Jacobian mattrix have negative real parts. The trajectory of the system (5.6) is a solution at time t starting at x, and it is denoted by $\phi(t,x)$. The stability region of an asymptotically stable equilibrium point (SEP) x_s can be expressed as [41]:

$$A(x_s) = \{x : \phi(t,x) \to x_s, \quad \text{as } t \to +\infty\} \tag{5.7}$$

To analyze transient stability due to a fault, the system is considered to go through three stages: pre-fault stage, fault-on stage and post-fault stage. The fundamental issue of transient stability analysis is whether the system trajectory, starting at the post-fault initial state $x(t_{cl})$, will settle down to x_s^{post}. In other words, transient stability analysis is to

determine whether the initial point of the post-fault trajectory is located inside the stability region of the equilibrium point x_s^{post}. It can be mathematically expressed by checking the following condition:

$$x(t_{cl}) \in A(x_s^{post}) \tag{5.8}$$

To be practical we need to consider a large set of contingencies. A large RTO in the East of U.S. evaluate about 3000 contingencies in on-line environments. Let N be the set of the contingencies being considered in a TSCOPF problem, and $A(x_{si}^{post})$ $i \in N$ denotes the stability region of x_{si}^{post} associated with contingency *i*. Then the mathematical expression of the transient stability constraints in TSCOPF based on the stability-region framework can be described as follows.

$$x_i(t_{cl}) \in A(x_{si}^{post}) \quad \forall i \in N \tag{5.9}$$

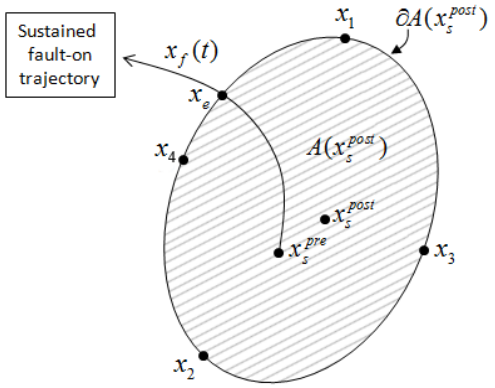

Figure 5-1: The fault-on trajectory $x_f(t)$, starting from the pre-fault SEP x_s^{pre}, moves toward the stability boundary $\partial A(x_s^{post})$ and intersects it at the exit point, x_e.

Solving a TSCOPF problem is challenging because the expression of transient stability constraints does not have a closed-form analytical expression. As a result, a predefined and fixed threshold for rotor angles of the following form has been popular to represent transient stability constraints

$$\begin{aligned} &\left|\delta_i(t) - \delta_{COI}(t)\right|_{\max} \le \delta_{\max} \\ &0 \le t \le t_{\max} \end{aligned} \tag{5.10}$$

where $\delta_i(t)$ is the rotor angle of machine *i* at time *t*. $\delta_{COI}(t)$ is the center of inertia (COI) reference angle. $\delta_{\max}$ is a fixed angle threshold, normally set between 100° - 120°. $t_{\max}$ is the time duration. In discretization-based TSCOPF, $t_{\max}$ is typically set to be between 2 and 5 seconds.

It can be shown that the exact threshold values are system-dependent, loading-condition-dependent and network-topology-dependent. The exact threshold values can vary from 80 to 190 degrees depending on several factors such as types of contingency, loading conditions, and network topology [40]. It is also shown that using the same fixed threshold for every contingency can lead to severe underestimated and overestimated stability assessments as well as degradations of the optimal solutions.

Therefore, it is strongly recommended that the following stability criterion (5.11) be adopted instead of (5.10):

$$\begin{aligned} &\left|\delta_i(t)-\delta_{COI}(t)\right|_{\max} \le \delta^j_{\max}(\mathbf{z}) \\ &0 \le t \le t_{\max} \qquad\qquad \forall j \in N \end{aligned} \tag{5.11}$$

where $\delta^j_{\max}(\mathbf{z})$ are the threshold values to be computed on the fly. These thresholds depend on the system control variables $\mathbf{z}$, and each contingency j and can be computed by the proposed method. The numerical discretization technique is applied to discretize the differential equations into a set of equivalent algebraic equations. Based on the equations (5.2)-(5.5) and (5.11), our TSCOPF formulation can then be described as follows:

$$\begin{aligned} \min_{\hat{\mathbf{x}},\mathbf{z}} \quad & f(\hat{\mathbf{x}},\mathbf{z}) \\ s.t. \quad & \mathbf{H}_1(\hat{\mathbf{x}},\mathbf{z}) = 0 \\ & \mathbf{G}_1(\hat{\mathbf{x}},\mathbf{z}) \le 0 \end{aligned} \tag{5.12}$$

where vector $\hat{\mathbf{x}}$ are the new state variables which includes all discretized state variables.

The difference between the proposed formulation and the traditional discretization-based TSCOPF formulation is the inclusion of accurate expression of transient stability criterion shown in (5.11) and a much less number of contingencies to be considered.

Instead of using the same fixed threshold value for every power system and for each contingency, we propose to compute on the fly the threshold values that reflect system's actual dynamics under study contingencies.

5.3 Controlling Unstable Equilibrium Point

Let x_s^{pre} be a pre-fault stable equilibrium point (SEP), $x_f(t)$ be the corresponding fault-on trajectory and x_s^{post} be the post-fault SEP. Let $\partial A(x_s^{post})$ denote the stability boundary of the post-fault SEP x_s^{post} . A comprehensive theory of stability boundary characterization of nonlinear systems has been developed in [43] and [44]. The exit point plays a direct relationship between the fault-on trajectory and the post-fault system as it uniquely defines the controlling unstable equilibrium point (CUEP).

Definition 1*:* (Exit-Point) Given a contingency on a power system stability model, the point at which the sustained fault-on trajectory intersects with the stability boundary of the post-fault SEP is called the *exit-point* of the fault-on trajectory (relative to the post-fault system). In addition, the fault-on trajectory exits the stability region after the exit point.

Definition 2*:* (CUEP) The CUEP of a fault-on trajectory $x_f(t)$ is the UEP whose stable manifold contains the exit point of $x_f(t)$ (i.e. the CUEP is the first UEP whose stable manifold intersects with the fault-on trajectory $x_f(t)$ at the exit point).

Theorem 1*:* (Existence and Uniqueness of the CUEP) Given a pre-fault SEP, a fault-on system, and a post-fault system with an SEP x_s^{post}. Let the post-fault system admit an energy function $V(\cdot): R^{2n} \to R$ and let the stability region of x_s^{post} contain the pre-fault SEP. Then, the CUEP of the fault-on trajectory always exists and is unique.

Proof*:* The existence of the exit point of a fault-on trajectory is ensured as long as the energy function value increases along the fault-on trajectory. This proof is built on the following facts.

1) A sustained fault-on trajectory must exit the stability boundary of a post-fault system.
2) The exit point of the fault-on trajectory must lie on the stable manifold of a UEP on the stability boundary of the post-fault system.

Fact 1) is a consequence of the following two conditions: (i) the fundamental assumption of direct methods that the pre-fault SEP lies inside the stability region of the post-fault SEP and (ii) the energy value increases along a fault-on trajectory. Fact 2) is a consequence of the following fundamental theorem [29]: the stability boundary is contained in the union of the stable manifolds of the UEPs on the boundary. Combining both facts, we complete the proof.

According to Theorem 1, the stable manifold of CUEP forms the relevant stability boundary toward which the fault-on trajectory moves. If the fault is cleared before the fault-on trajectory reaches the relevant stability boundary, then the post-fault system will be stable; otherwise, it will be unstable. Hence, the CUEP method for direct analysis of transient stability is composed of the following two tasks: (i) compute the CUEP relevant to the fault-on trajectory, and (ii) approximate the stable manifold of the CUEP by the constant energy surface passing through the CUEP.

In this chapter, the BCU method [46] is adopted to compute CUEPs and perform direct analysis of system transient stability. The BCU method plays a vital role in our proposed BCU-based TSCOPF methods by providing a fast assessment and screening tool, and assisting in the computation of system threshold values.

5.4 A BCU-Based Scheme for Computing Threshold

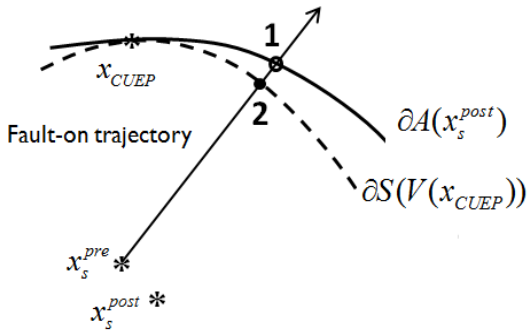

Figure 5-2: Visualization of two initial points for computing system thresholds. Point 1 can be computed by time-domain-based while Point 2 by the proposed CUEP-based scheme. System thresholds computed from point 1 leads to an exact value while the results computed from point 2 are estimated and conservative values.

Figure 5-2 illustrates the main differences between the time-domain-based method and BCU-based methods in computing system threshold values. To obtain an exact threshold, a post-fault trajectory starting from a point lying just inside the stability boundary (point 1) must be computed and analyzed [40]. This exact point however can be very expensive to compute due to the requirement of locating the exact relevant stability boundary in the direction of the fault-on trajectory. This usually requires several numerical integrations of the post-fault system. On the other hand, the CUEP method approximates the relevant stability boundary and computes point 2 as an approximation of point 1. This scheme is much faster than the time-domain-based approach due to the direct identification of the initial point 2 (for computing system thresholds) via the constant energy surface passing through the CUEP. A comprehensive theoretical foundation of CUEP has been developed in [45,50] The proposed scheme is presented as follows:

Given: A contingency with a specified fault-on trajectory and a specified post-fault SEP.

Method: Computing accurate threshold values for angle inequalities in the form of (5.11).

Step 1: Compute the CUEP, x_{CUEP}, relative to the fault-on trajectory using the BCU method.

Step 2: Find the point along the fault-on trajectory that crosses the constant energy surface passing through the CUEP.

Step 3: Perform a time-domain numerical integration starting from the point computed in step 2. (This step produces an estimated critically stable post-fault trajectory.)

Step 4: Identify the maximum angle deviation $\delta_{\max}^{est}$ along the critically stable post-fault trajectory, which can be found at the highest or lowest peak of the trajectories.

Output: The estimated threshold value of the contingency in the context of angle inequality is $\delta_{\max}^{est}$.

Table 5-1: Exact (Time-domain) vs. Estimated (BCU) Threshold Values

Contingencies	TD-based Exact Threshold (degree)	BCU-based Estimated Threshold (degree)	Relative Error %
Secure	CCT > 0.2		
59: 59-72	174.24	164.11	5.81
116:115-116	192.63	173.3	10.03
1: 1-2	176.47	172.09	2.48
8: 7-8	165.81	151.67	8.53
11: 9-11	172.69	165.7	4.05
Critical	0.1 < CCT <0.2		
6: 7-6	190.11	188.41	0.89
7:7-6	182.66	175.52	3.91
104: 7-104	195.03	175.28	10.13
98: 58-98	144.10	140.34	2.61
89: 59-89	155.10	143.08	7.75
Insecure	CCT < 0.1		
17: 17-22	139.74	133.32	4.59
33: 33-34	115.22	110.47	4.12
99: 36-99	110.70	99.01	10.56
2: 2-113	113.45	104.52	7.87

Table 5-2: Exact (Time-domain) vs. Estimated (BCU) CPU Time

Contingencies	TD-based CPU time (sec)	BCU-based CPU time (sec)	Relative improvement %
Secure	CCT > 0.2		
59: 59-72	132.48	15.23	88.50393
116:115-116	156.22	16.09	89.70042
1: 1-2	142.48	12.23	91.41634
8: 7-8	135.23	12.1	91.05228
11: 9-11	149.01	17.64	88.16187
Critical	0.1 < CCT <0.2		
6: 7-6	128.46	13.35	89.60766
7:7-6	148.1	15.48	89.5476
104: 7-104	132.09	11.29	91.4528
98: 58-98	133.67	12.31	90.79075
89: 59-89	143.59	16.75	88.33484
Insecure	CCT < 0.1		
17: 17-22	153.27	11.04	92.79702
33: 33-34	147.48	13.58	90.79197
99: 36-99	139.95	12.02	91.41122
2: 2-113	131.3	14.6	88.88043

The proposed scheme has been evaluated on several test cases. Parts of the evaluation results are summarized in Table 5-1 and Table 5-2. The tests were performed on three groups of contingencies based on their level of severity. In Table 5-2, it can be seen that the estimated thresholds are uniformly and slightly smaller than the exact threshold values. The average relative error from all 14 cases is 5.95%. Table 5-2 shows the comparison of CPU time between two approaches. It is clear that the computational times by the proposed BCU-based scheme are much less than the original time-domain-based approach. The average relative improvement for CPU time is 90.17%. Although the computation has been greatly reduced due to the approximation, the system thresholds estimated by the proposed scheme still reflects the network topology, loading conditions, etc. and is based on the concept of relevant stability boundary of nonlinear systems [50].

From these numerical studies of the BCU-based scheme, we obtained the following observations:

(1) The threshold values estimated by the proposed scheme are slightly smaller than the exact threshold values, with very small relative errors.

(2) The threshold values estimated by the proposed scheme are always less than the exact threshold values. This shows the slightly conservative nature of the proposed scheme.

(3) The BCU-based scheme is much faster than the time-domain approach in computing threshold values.

(4) The conventional TSCOPF guideline with a fixed 100° threshold is too conservative for all cases in Table 5-1.

5.5 Proposed BCU-based TSCOPF Method

The proposed BCU-based TSCOPF method is presented in Figure 5-3. The method has the following key steps:

1. Assessment and screening step (contingency reduction step)
2. Calculation of accurate threshold value step (threshold value calculation for each critical contingency)
3. Reduced-size TSCOPF problem formulation
4. Solving the reduced-size TSCOPF problem

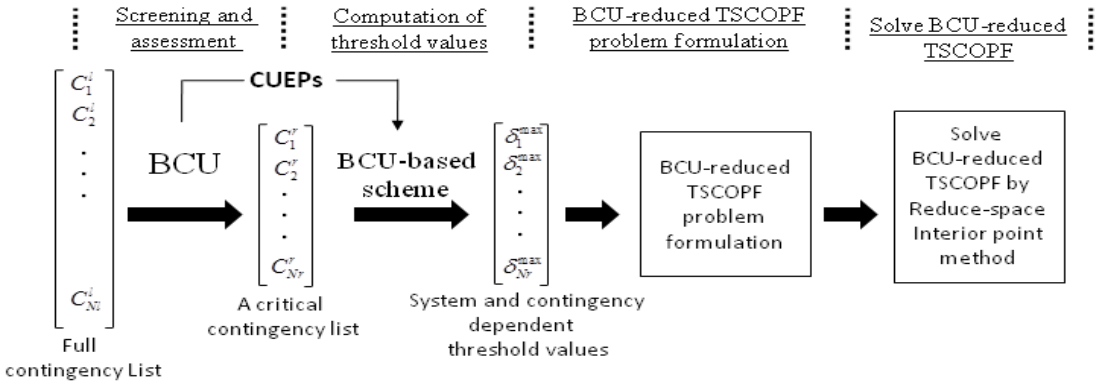

Figure 5-3: The conceptual BCU-based TSCOPF method for large-scale power systems with large contingency lists. The method consists of (i) fast assessment and screening by BCU method for taking out irrelevant contingencies (ii) computation of system and contingency dependent threshold values via a BCU-base scheme, (iii) Reduce-space interior point method.

1) Assessment and screening

Practical large-scale power systems are subject to large contingency lists, but typically only a few contingencies are indeed insecure and critical, and require preventive control actions. Due to the computation limitation of numerical discretization-based TSCOPF, it is important not to include a large number of contingencies in the formulation. To help a large number of secure contingencies from getting included in the main TSCOPF solver, the BCU method is incorporated as a fast screening tool. This ensures that only critical or insecure contingencies are included in the TSCOPF formulation. As a result, a large-size contingency list is then reduced to a much smaller size of critical contingency list.

2) Computation of accurate threshold values

The importance of using accurate threshold values in (5.11) has been stressed in [40]. The proposed BCU-based scheme is implemented to compute accurate system threshold for each critical or insecure contingency. One advantage of using this scheme as a screening tool is that, the CUEPs are already computed in the screening process, and hence can be readily used by the scheme.

3) Reduced-size TSCOPF formulation

The BCU-based TSCOPF formulation is formed by enforcing the angle-limit inequalities only for the critical and insecure contingencies. The threshold values computed by the BCU-based time-domain scheme are used as accurate threshold values.

4) Solving the reduced-size TSCOPF

The reduced-space interior point method [37] is applied to solve the BCU-reduced TSCOPF formulation.

The flow chart of the proposed BCU-based TSCOPF method which includes a computational loop that constantly checks and updates the system contingency list and threshold values is shown in Figure 5- 4. We begin this procedure by solving a standard

OPF. The BCU method is then executed to screen out secure cases and to calculate CUEPs for computing accurate threshold values of critical contingencies. Once the threshold values are computed, the main TSCOPF solver is executed to solve the BCU-reduced TSCOPF problem. This process repeats until no insecure contingency is found. The procedure is described as follows:

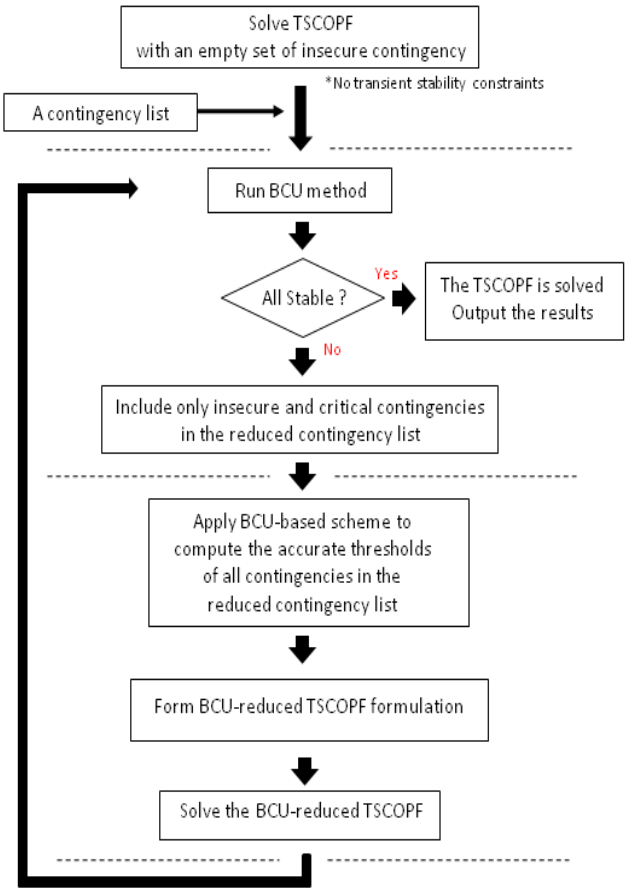

Figure 5-4: The flow chart of the BCU-based OPF method for solving large-scale TSCOPF problems with a large-size contingencies.

Given: A power system case with a contingency list.

Method: Computing TSCOPF solution based on the proposed BCU-based scheme.

Step 1: Solve standard OPF without considering any transient stability constraints.

Step 2: Run BCU method to filter out screen out secure cases. Save the CUEPs of insecure and critical cases.

Step 3: Check if all contingencies are secure. If yes, end the program and output solution, otherwise proceed to step 4.

Step 4: Include all insecure and critical contingencies in the reduced contingency list

Step 5: Compute the accurate threshold value of each insecure and critical contingency in the reduced contingency list using the proposed BCU-based scheme.

Step 6: Form the BCU-reduced TSCOPF formulation in expression (5.12) using the threshold values computed in step 5.

Step 7: Solve the BCU-reduced TSCOPF formulation using the reduced-state interior point method and repeat step 2.

Output: A transient stability constrained optimal power flow solution.

5.6 Case Studies

In order to evaluate the robustness and efficiency of the proposed BCU-based method, detailed numerical results for different test systems are presented in this section. Table 5-3gives a summary of these test systems.

Table 5-3: Summary of All Test Systems

Test Systems	N_B	N_G	$T_{\max}$ (SEC)	Δt
WSCC9	9	3	2.00	0.01
IEEE39	39	10	2.00	0.02
IEEE145	145	50	2.00	0.02
IEEE162	162	25	2.00	0.02
IEEE300	300	69	2.00	0.02
CASE678	678	170	2.00	0.02

*NB = Number of buses, NG = Number of generators
Tmax = Total integration time, Δt = integration step size

In realistic scenarios, it is inevitable that large numbers of contingencies must be considered when TSCOPF problems are solved. Without a fast screening tool, it can be extremely expensive or impossible to perform the TSCOPF computation. Table 5-4 shows the screening performance of the BCU method in eliminating irrelevant or stable contingencies. The accuracy of the BCU method is confirmed by the time-domain simulation program. Although a small number of secure cases did not get screened out, it is due to the slightly conservative nature of the CUEP method. Moreover, the computation times taken by the BCU method are much less when compared to the traditional time-domain approach. This confirms that the BCU method can greatly reduce the number of contingencies to be included in the main TSCOPF formulation.

Table 5-4: BCU Classifiers and Screening performance

System	Nl	Contingency screening		
		BCU method Drop-out cases	Time-Domain stable cases	BCU Screening Rate %
WSCC9	10	8	8	100
IEEE39	50	45	46	97.83
IEEE145	300	293	295	99.32
IEEE162	300	295	297	99.33
IEEE300	300	298	299	99.67
CASE678	300	298	298	100

*Nl is number of contingencies in the contingency list

Table 5-5: Capability to handle large contingency lists Conventional TSCOPF 100° (IPM) vs. BCU-based TSCOPF (IPM)

System	*Nl	CPU time (sec)		
		Conventional TSCOPF 100° (IPM)	Conventional TSCOPF 100° (IPM) *with TD screening	BCU-based TSCOPF (IPM)
WSCC9	10	4.759	8.41	4.623
IEEE39	50	-	40.33	21.06
IEEE145	300	-	1256.45	538.42
IEEE162	300	-	2696.78	1002.59
IEEE300	300	-	4073.19	1716.44
CASE678	300	-	14493.05	6128.81

*Nl is number of contingencies in the contingency list

** Post-fault numerical integration of 5 seconds is used to assess transient stability.

Table 5-6: TSCOPF Solution Quality Fixed threshold 100° vs. Computed Thresholds (BCU-based)

System	Nl	Objective function value at TSCOPF solution		Relative improvement %
		Conventional TSCOPF 100° (IPM) *with TD screening	BCU-based TSCOPF (IPM)	
WSCC9	10	$15,421	$14,031	9.01%
IEEE39	50	$65,330	$61,248	6.25%
IEEE145	300	$203,449	$185,226	8.96%
IEEE162	300	$148,405	$132,110	10.98%
IEEE300	300	$544,095	$523,060	3.87%
CASE678	300	$832,713	$790,432	5.08%

*Nl is number of contingencies in the contingency list

Table 5-5 provides a comparison summary of the OPF solutions obtained by the conventional method and by the proposed BCU-based TSCOPF with a focus on the capability in handling large contingency lists. Both methods utilize interior point method as the main TSCOPF solver. The third and fifth columns show that the conventional approach cannot solve most of the cases while the BCU-based approach is successful in all cases, including 678-bus system with 300 contingencies. Forth column of Table 5-5 presents the CPU time when conventional TSCOPF is performed along with a time-domain-based approach for screening. It can be seen that the CPU times by the time-domain approach are much higher than the BCU-based approach in all cases. This inferior performance in computational speed by the time-domain approach is mainly caused by the time-consuming numerical integrations of post-fault systems.

The advantage of using accurate system threshold values is presented in Table 5-6. The widely-used fixed threshold proxi with 100° is utilized by the conventional TSCOPF (with TD screening). We note that the BCU-based TSCOPF method computes and uses the actual system threshold values. The results show that by using more accurate threshold values, the quality of the optimal solutions of all test systems is greatly improved. The resulting objective function values of total generation costs are shown in the Table 5-6. The average improvement on the objective function values is 7.03%.

5.7 Conclusions

The TSCOPF problem is indeed a challenging optimization one. A BCU-based method is proposed for computing solutions of large-scale TSCOPF problems with a large set of contingencies. Details of the BCU-based method are discussed, including the BCU-based scheme for computing accurate system thresholds and the implementation of the BCU method as fast screening tool. The key features of the proposed BCU-based TSCOPF method are as follows:

1) The BCU method provides a fast and effective tool to screen out irrelevant or secure contingencies. This capability greatly reduces the required computational burden when large contingency lists are considered.

2) The BCU-based method for computing system threshold values provides the TSCOPF solver with accurate system-dependent threshold values. This improves both the accuracy in stability assessment and the quality of the TSCOPF solution.

3) This BCU-based method is applicable to any discretization based TSCOPF solvers.

Numerical results on several TSCOPF problems indicated that the proposed BCU-based method improves (i) the computational speed, (ii) the capability of TSCOPF method to handle large contingency lists, (iii) the accuracy of transient stability constraint in TSCOPF formulation, and (iv) the quality of optimal solutions of every test system. These promising results suggest that the proposed method can be an effective alternative for solving large-scale TSCOPF with large contingency lists.

References

[1] R. D. Zimmerman, C. E. Murillo-Sánchez, and R. J. Thomas, "MATPOWER: Steady-State Operations, Planning and Analysis Tools for Power Systems Research and Education," *Power Systems, IEEE Transactions on*, vol. 26, no. 1, pp. 12-19, Feb. 2011. 2

[2] R. D. Zimmerman, C. E. Murillo-Sánchez, and R. J. Thomas, "MATPOWER's Extensible Optimal Power Flow Architecture," *Power and Energy Society General Meeting, 2009 IEEE*, pp. 1-7, July 26-30 2009. 2

[3] R. D. Zimmerman and C. E. Murillo-Sánchez, MATPOWER User's Manual, [Online]. Available: http://www.pserc.cornell.edu/matpower/ 2

[4] C. Murillo-Sánchez, R. Zimmerman, C. Anderson, and R. Thomas, "A stochastic, contingency-based securit-constrained optimal power flow for the procurement of energy and distributed reserve," *Decision Support Systems*, 2013, http://dx.doi.org/10.1016/j.dss.2013.04.006.

[5] C. Murillo-Sanchez, R. Zimmerman, C. Anderson, and R. Thomas, "Secure Planning and Operations of Systems with Stochastic Sources, Energy Storage, and Active Demand", *Smart Grid, IEEE Transactions on*, 4(4):2220-2229, 2013.

[6] Gan D., Thomas R. J., Zimmerman R. D., "Stability-constrained optimal power flow," *IEEE Transactions on Power Systems* , vol.15, no.2, pp.535-540, May 2000.

[7] Chen L., Tada Y., Okamoto H., Tanabe R., Ono A.; , "Optimal operation solutions of power systems with transient stability constraints," *IEEE Transactions on Circuits and Systems I: Fundamental Theory and Applications* , vol.48, no.3, pp.327-339, Mar 2001.

[8] La Scala M., Trovato M., Antonelli C., "On-line dynamic preventive control: an algorithm for transient security dispatch," *IEEE Transactions on Power Systems*, vol.13, no.2, pp.601-610, May 1998.

[9] De Tuglie E., Dicorato M., La Scala M., Scarpellini P., "A static optimization approach to assess dynamic available transfer capability," *IEEE Transactions on Power Systems*, vol.15, no.3, pp.1069-1076, Aug 2000.

[10] Yue Yuan, Kubokawa, J., Sasaki, H., "A solution of optimal power flow with multicontingency transient stability constraints," , *IEEE Transactions on Power Systems* , vol.18, no.3, pp. 1094- 1102, Aug. 2003

[11] Tangpatiphan K., Yokoyama A., "Adaptive Evolutionary Programming with Neural Network for Transient Stability Constrained Optimal Power Flow," *Intelligent*

System Applications to Power Systems, 2009. ISAP '09. 15th International Conference on , vol., no., pp.1-6, 8-12 Nov. 2009.

[12] Mo N., Zou Z.Y., Chan K.W., Pong T.Y.G., "Transient stability constrained optimal power flow using particle swarm optimisation," *Generation, Transmission & Distribution, IET* , vol.1, no.3, pp.476-483, May 2007.

[13] Hakim L., Kubokawa J., Yue Yuan, Mitani T., Zoka Y., Yorino N., Niwa Y., Shimomura K., Takeuchi A., "A Study on the Effect of Generation Shedding to Total Transfer Capability by Means of Transient Stability Constrained Optimal Power Flow," *Power Systems, IEEE Transactions on* , vol.24, no.1, pp.347-355, Feb. 2009.

[14] Quanyuan Jiang, Guangchao Geng, "A Reduced-Space Interior Point Method for Transient Stability Constrained Optimal Power Flow," *IEEE Transactions on Power Systems*, vol.25, no.3, pp.1232-1240, Aug. 2010.

[15] Quanyuan Jiang, Zhiguang Huang, "An Enhanced Numerical Discretization Method for Transient Stability Constrained Optimal Power Flow," *IEEE Transactionson Power Systems*, vol.25, no.4, pp.1790-1797, Nov. 2010.

[16] Xiaojiao Tong, Wei He, Renjun Zhou, Xuehua Deng, "Calculation for optimal power flow with transient stability constraints based on semi-infinite programming algorithm," *Power and Energy Society General Meeting*, pp.1-6, 20-24 July 2008.

[17] H-D Chiang, Y. Tada, H. Li, "Power System On-line Transient Stability Assessment", in *Wiley Encyclopedia of Electrical and Electronics Engineering*. JohnWiley & Sons, Inc., 2008

[18] H. D. Chiang, C. C. Chu, and G. Cauley, "Direct stability analysis of electric power systems using energy functions: Theory, applications and perspective (Invited paper)", *Proceedings of the IEEE*, Vol. 83, No. 11, Nov. 1995.

[19] H. D. Chiang, M. W. Hirsch, and F. F. Wu, "Stability regions of non-linear autonomous dynamical systems," *IEEE Trans. on Automatic Control*, vol. 33, no. 1, pp. 16-27, Jan 1988.

[20] H. D. Chiang and J. S. Thorp, "Stability regions of nonlinear dynamical systems: a constructive methodology" *IEEE Trans. on Automatic Control*, vol. 34, no. 12, Dec. 1989.

[21] P. Kundur, *Power System Stability and Control.*, New York: McGraw-Hill, 1994.

[22] P. W. Sauer, and M. A. Pai, "Power Systems Dynamics and Stability," 1998, pp. 171.

[23] Hsiao-Dong Chiang, *Direct Methods for Stability Analysis of Electric Power Systems: Theoretical Foundation, BCU Methodologies, and Applications*, Wiley, New Jersey, 2011

[24] R. D. Zimmerman and D. Gan, “MATPOWER, a MATLAB power system simulation package,” Power System Engineering Research Center, Cornell Univ., Ithaca, NY, 1997.

[25] Brian Stott, Eric Hobson, "Power System Security Control Calculations Using Linear Programming, Part I," IEEE Transactions on Power Apparatus and Systems, vol.PAS-97, no.5, pp.1713-1720, Sept. 1978

[26] Y.C. Wu, A. S. Debs, and R. E. Marsten, “A direct nonlinear predictor-corrector primal-dual interior point algorithm for optimal power flows,” IEEE Trans. Power Syst., vol. 9, no. 2, pp.876-883, May 1994.

[27] H. Wei, H. Sasaki, J. Kubokawa, and R. Yokoyama, “An interior point nonlinear programming for optimal power flow problems with a novel data structure,” IEEE Trans. Power Syst., vol. 13, no. 3, pp. 870–877, Aug. 1998.

[28] Gan D., Thomas R. J., Zimmerman R. D., "Stability-constrained optimal power flow," IEEE Transactions on Power Systems , vol.15, no.2, pp.535-540, May 2000.

[29] Chen L., Tada Y., Okamoto H., Tanabe R., Ono A.; , "Optimal operation solutions of power systems with transient stability constraints," IEEE Transactions on Circuits and Systems I: Fundamental Theory and Applications , vol.48, no.3, pp.327-339, Mar 2001.

[30] La Scala M., Trovato M., Antonelli C., "On-line dynamic preventive control: an algorithm for transient security dispatch," IEEE Transactions on Power Systems, vol.13, no.2, pp.601-610, May 1998.

[31] De Tuglie E., Dicorato M., La Scala M., Scarpellini P., "A static optimization approach to assess dynamic available transfer capability," IEEE Transactions on Power Systems, vol.15, no.3, pp.1069-1076, Aug 2000.

[32] Yue Yuan, Kubokawa, J., Sasaki, H., "A solution of optimal power flow with multicontingency transient stability constraints," , IEEE Transactions on Power Systems , vol.18, no.3, pp. 1094- 1102, Aug. 2003

[33] Tangpatiphan K., Yokoyama A., "Adaptive Evolutionary Programming with Neural Network for Transient Stability Constrained Optimal Power Flow," Intelligent System Applications to Power Systems, 2009. ISAP '09. 15th International Conference on , vol., no., pp.1-6, 8-12 Nov. 2009.

[34] Mo N., Zou Z.Y., Chan K.W., Pong T.Y.G., "Transient stability constrained optimal power flow using particle swarm optimisation," Generation, Transmission & Distribution, IET , vol.1, no.3, pp.476-483, May 2007.

[35] Hakim L., Kubokawa J., Yue Yuan, Mitani T., Zoka Y., Yorino N., Niwa Y., Shimomura K., Takeuchi A., "A Study on the Effect of Generation Shedding to Total Transfer Capability by Means of Transient Stability Constrained Optimal Power Flow," Power Systems, IEEE Transactions on , vol.24, no.1, pp.347-355, Feb. 2009.

[36] Quanyuan Jiang, Guangchao Geng, "A Reduced-Space Interior Point Method for Transient Stability Constrained Optimal Power Flow," IEEE Transactions on Power Systems, vol.25, no.3, pp.1232-1240, Aug. 2010.

[37] Quanyuan Jiang, Zhiguang Huang, "An Enhanced Numerical Discretization Method for Transient Stability Constrained Optimal Power Flow," IEEE Transactionson Power Systems, vol.25, no.4, pp.1790-1797, Nov. 2010.

[38] Xiaojiao Tong, Wei He, Renjun Zhou, Xuehua Deng, "Calculation for optimal power flow with transient stability constraints based on semi-infinite programming algorithm," Power and Energy Society General Meeting, pp.1-6, 20-24 July 2008.
[39] W. Suampun, H.-D. Chiang, "Evaluation Study of the Incorporation of Transient Stability Constraints into Optimal Power Flow," IEEE Transactions on Power Systems
[40] H.-D. Chiang, Y. Tada, H. Li, "Power System On-line Transient Stability Assessment", in Wiley Encyclopedia of Electrical and Electronics Engineering. JohnWiley & Sons, Inc.
[41] H.-D. Chiang, C. C. Chu, and G. Cauley, "Direct stability analysis of electric power systems using energy functions: Theory, applications and perspective (Invited paper)", Proceedings of the IEEE, Vol. 83, No. 11, Nov. 1995.
[42] H.-D. Chiang, M. W. Hirsch, and F. F. Wu, "Stability regions of non-linear autonomous dynamical systems," IEEE Trans. on Automatic Control, vol. 33, no. 1, pp. 16-27, Jan 1988.
[43] H.-D. Chiang and J. S. Thorp, "Stability regions of nonlinear dynamical systems: a constructive methodology" IEEE Trans. on Automatic Control, vol. 34, no. 12, Dec. 1989.
[44] H.-D. Chiang, F. F. Wu, P. P. Varaiya, "Foundations of direct methods for power system transient stability analysis," IEEE Transactions on Circuits and Systems, vol.34, no.2, pp. 160- 173, Feb 1987
[45] H.-D. Chiang, E F. Wu and P. P. Varaiya, "A BCU Method for Direct Analysis of Power System Transient Stability", IEEE Transactions on Power Systems, vol. 8, no.3, Aug., pp. 1194-1208, 1994.
[46] Hsiao-Dong Chiang; Cheng-Shan Wang; Hua Li, "Development of BCU classifiers for on-line dynamic contingency screening of electric power systems," IEEE Transactions on Power Systems , vol.14, no.2, pp.660-666, May 19.
[47] P. Kundur, Power System Stability and Control., New York: McGraw-Hill, 1994.
[48] P. W. Sauer, and M. A. Pai, "Power Systems Dynamics and Stability," 1998, pp. 171.
[49] Hsiao-Dong Chiang, Direct Methods for Stability Analysis of Electric Power Systems: Theoretical Foundation, BCU Methodologies, and Applications, Wiley, New Jersey, 2011
[50] R. D. Zimmerman and D. Gan, "MATPOWER, a MATLAB power system simulation package," Power System Engineering Research Center, Cornell Univ., Ithaca, NY, 1997.